Phase Noise in *LC* Oscillators: A Phasor-Based Analysis of a General Result and of Loaded Q

David Murphy, *Student Member, IEEE*, Jacob J. Rael, *Member, IEEE*, and Asad A. Abidi, *Fellow, IEEE*

***Abstract*—Recent work by Bank, and Mazzanti and Andreani has offered a general result concerning phase noise in nearly-sinusoidal inductance–capacitance (*LC*) oscillators; namely that the noise factor of such oscillators (under certain achievable conditions) is largely independent of the specific operation of individual transistors in the active circuitry. Both use the impulse sensitivity function (ISF). In this work, we show how the same result can be obtained by generalizing the phasor-based analysis. Indeed, as applied to nearly-sinusoidal *LC* oscillators, we show how the two approaches are equivalent. We analyze the negative-gm *LC* model and present a simple equation that quantifies output noise resulting from phase fluctuations. We also derive an expression for output noise resulting from *amplitude* fluctuations. Further, we extend the analysis to consider the voltage-biased *LC* oscillator and fully differential CMOS *LC* oscillator, for which the Bank's general result does not apply. Thus we quantify the concept of loaded Q.**

***Index Terms*—Impulse sensitivity function, noise factor, oscillators, voltage controlled oscillator, phase noise.**

I. Introduction

THE PAST 20 years have seen significant progress in the understanding of noise in electrical oscillators. During this period, the design community has advanced beyond Leeson's classic linear analysis [1] and adopted analysis methods that more appropriately capture the time-varying and large-signal nature of any realizable oscillator. While lacking the rigor of mathematically involved analyses [2]–[4], the linear-time variant (LTV) approach to analyzing noise in oscillators has gained the most traction in the circuit design community. This is no doubt attributable to the high accuracy of its predictions and the relative simplicity of the mathematical tools employed. Two LTV methods stand out: the impulse-response-based approach proposed by Hajimiri and Lee [5], [6], and the phasor-based approach pioneered by Samori *et al.* [7], Huang [8], and Rael and Abidi [9].

Central to Hajimiri and Lee's work is the derivation of the impulse sensitivity function (ISF) that shows how the phase disturbance produced by a current impulse depends on the time at which the impulse is injected; for example, a current impulse injected at a zero-crossing will generate a greater phase shift than if injected at the peak of an oscillation. The work is very intuitive and, if applied correctly, results in accurate predictions;

Manuscript received April 20, 2009; revised July 08, 2009; accepted July 13, 2009. First published December 18, 2009; current version published June 09, 2010.

D. Murphy and A. A. Abidi are with the Electrical Engineering Department, University of California, Los Angeles, CA 90095 USA (e-mail: dmurphy@ee.ucla.edu).

J. J. Rael is with Broadcom Corporation, Irvine, CA 92617 USA (e-mail: jjrael@broadcom.com).

Digital Object Identifier 10.1109/TCSI.2009.2030110

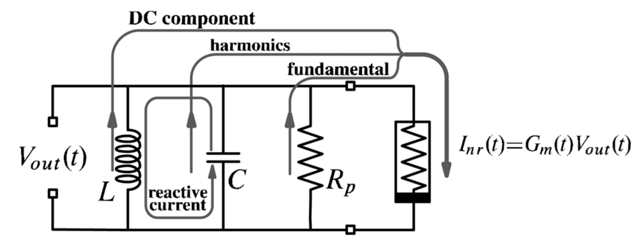

Fig. 1. Generic negative-gm *LC* oscillator model.

notably Andreani *et al.* [10]–[13] have used the ISF to develop closed form expressions for the most common inductance–capacitance (*LC*) oscillators. More recently, Bank [14] used the ISF to derive a remarkable result, namely that the noise factor of a nearly-sinusoidal *LC* oscillator, under certain common conditions, is largely independent of the specific operation of individual transistors in the active circuitry. Mazzanti and Andreani [15] then, aware of Bank's work, provided a novel proof of this same general result. Their work also employed the ISF.

The alternative phasor-based analysis method, which is adopted in [7], [9], [16], [17], looks at phase noise generation mechanisms in the frequency domain. While this approach is practical only for nearly-sinusoidal *LC* oscillators, it offers an alternative perspective and does not require the development of specific theoretical concepts such as Hajimiri and Lee's ISF. Nevertheless, published work expanding on this method appears curiously to have dried up after Kouznetsov and Meyer [16]. As in the ISF approach, all noise sources are considered stationary or cyclostationary (with respect to the oscillation frequency) [18], and both calculations involve a given source acting on a "noiseless" oscillator. Thus one would expect that the two approaches would yield the same results, with neither approach exhibiting an obvious advantage over the other. In this paper, we are able to show that this is, indeed, the situation.

Building our group's previous results [9], [17], [19], and drawing from the work of Samori *et al.* [7], we re-derive the general result using phasor-based analysis, which does not rely on the ISF. In doing so, we reconcile the two widely cited approaches (ISF and phasor-based) and show how they are fundamentally the same[1]; both approaches result in equivalent expressions and suffer the same limitations. We focus on the negative-gm *LC* model (see Fig. 1), for which we present simple equations that quantify output noise resulting from phase fluctuations. Moreover, we derive a closed form expression for output noise arising from *amplitude* fluctuations, something the ISF approach has so far failed to do. Finally, we show how the analysis can be extended to account for topologies, such as

[1]As applied to phase fluctuations in *LC* oscillators.

1549-8328/$26.00 © 2010 IEEE

the voltage-biased oscillator, for which the general result is not applicable. This enables us to gain insight into tank loading and derive equations to quantify Q degradation.

Section II introduces the negative-gm model, and outlines our approach.

II. Oscillator Preliminaries

A. Negative-gm Oscillator

A nearly-sinusoidal *LC* oscillator can be modeled as a lossy resonator in parallel with an energy-restoring nonlinearity, as shown in Fig. 1. Assuming oscillation conditions are satisfied, Leeson [1] describes the output noise PSD resulting from phase fluctuations as

$$\widehat{v_{n_{\mathrm{PM}}}^2} = 2kTFR_p\left(\frac{\omega_0}{2Q\omega_m}\right)^2 \tag{1}$$

where Q is the quality factor of the resonator, ω_0 is the oscillation frequency, and ω_m is a frequency offset from ω_0. The noise factor F, left unspecified by Leeson, is the focus of this work. Leeson assumes that output noise arising from amplitude fluctuations, $\widehat{v_{n\mathrm{AM}}^2}$, is negligible.

Phase noise is defined as the total single-sideband output noise normalized to the power in the oscillator's sinusoidal output, i.e.,

$$\mathcal{L}\{\omega_m\} = \frac{\widehat{v_n^2}}{A_c^2/2} = \frac{\widehat{v_{n_{\mathrm{PM}}}^2} + \widehat{v_{n_{\mathrm{AM}}}^2}}{A_c^2/2} \tag{2}$$

where A_c is the oscillation amplitude.[2]

Employing the quasi-sinusoidal approximation [20], any single-phase nearly-sinusoidal *LC* topology can be redrawn (by means of a Norton or Thevenin transformation) in the form of this negative-gm *LC* model. This approximation also allows us to refer every noise source (cyclostationary or stationary) to an appropriate current noise source that appears differentially across the model's resonator. These manoeuvres are permissible because tones and noise at other frequencies are significantly attenuated by the resonator and so do not contribute to the output.[3]

Given this simplification, our approach is as follows: two transfer functions are derived that map a small AM or a PM resonator-referred current source to the oscillator's output (see Section III). We then show, in Section IV, how an arbitrary cyclostationary white noise source can be decomposed into its AM and PM components, which can make use of these transfer functions. In Section V, we apply this theory to the negative-gm *LC* model to generate expressions for output noise; in doing so, we quantify F and rederive the Bank's general result [14]. These expressions are applied to well-known topologies in Section VI. Section VII deals with topologies where the general result is not applicable.

We conclude this section by looking at the energy conservation requirement of an *LC* oscillator, which will be used to simplify later analysis.

B. Constraints From Energy Conservation

To sustain oscillation, the average power dissipated in the lossy tank must equal the average power delivered to the tank by the nonlinearity, i.e.,

$$\frac{1}{T}\int_{-\frac{T}{2}}^{\frac{T}{2}} P_{\mathrm{tank}}(t)dt = -\frac{1}{T}\int_{-\frac{T}{2}}^{\frac{T}{2}} P_{\mathrm{nr}}(t)dt \tag{3}$$

where $P_{\mathrm{tank}}(t)$ is the instantaneous power dissipated in the lossy tank, and $P_{\mathrm{nr}}(t)$ is the instantaneous power dissipated in nonlinearity. The instantaneous conductance of the nonlinearity is defined as

$$G_m(t) = \frac{dI_{\mathrm{nr}}(t)}{dV_{\mathrm{out}}(t)} = \frac{dI_{\mathrm{nr}}(t)}{dt}\frac{dt}{dV_{\mathrm{out}}(t)}. \tag{4}$$

Using this expression, and assuming the output is of the form $V_{\mathrm{out}} = A_c\cos(\omega_0 t)$, the current drawn by the nonlinearity can be described as

$$\begin{aligned} I_{\mathrm{nr}}(t) &= I_{\mathrm{nr_{DC}}} + \int_{-\infty}^{t} G_m(\tau)\frac{dV_{\mathrm{out}}(\tau)}{d\tau}\,d\tau \\ &= I_{\mathrm{nr_{DC}}} - \omega_0 A_c\int_{-\infty}^{t} G_m(\tau)\sin(\omega_0\tau)\,d\tau \end{aligned} \tag{5}$$

and the average power dissipated by the nonlinearity is

$$\begin{aligned} \langle P_{\mathrm{NR}}\rangle &= \frac{1}{T}\int_{-\frac{T}{2}}^{\frac{T}{2}} V_{\mathrm{out}}(t)I_{\mathrm{nr}}(t)\,dt \\ &= \frac{-\omega_0 A_c^2}{T}\int_{-\frac{T}{2}}^{\frac{T}{2}}\cos(\omega_0 t)\left(\int_{-\infty}^{t} G_m(\tau)\sin(\omega_0\tau)\,d\tau\right)dt. \end{aligned} \tag{6}$$

If we switch the order of the integrals, we may write

$$\begin{aligned} \langle P_{\mathrm{NR}}\rangle &= -\frac{\omega_0 A_c^2}{T}\int_{-\frac{T}{2}}^{\frac{T}{2}}\int_{\tau}^{\frac{T}{2}}\cos(\omega_0 t) \\ &\qquad\times G_m(\tau)\sin(\omega_0\tau)\,dt\,d\tau \\ &= \frac{A_c^2}{2T}\int_{-\frac{T}{2}}^{\frac{T}{2}} G_m(\tau)(1-\cos(2\omega_0\tau))\,d\tau. \end{aligned} \tag{7}$$

It is assumed that the nonlinearity is purely resistive and thus memoryless. Any memoryless nonlinear resistance excited by a zero-initial-phase cosine wave, as in this case, will produce an output that is a real and even function of time. Accordingly, the above expression may be written as

$$\langle P_{\mathrm{NR}}\rangle = \frac{A_c^2}{2}(G_M[0] - G_M[2]) \tag{8}$$

[2]Output noise consists of two components: output noise due to phase fluctuations and output noise due to *amplitude* fluctuations. As such, the term "phase noise" is somewhat of a misnomer as it is a measure of normalized output noise. However, this ambiguity is generally unimportant, since noise resulting from amplitude fluctuations is generally small at close-in offsets.

[3]This approach is similar to that adopted by Kouznetsov and Meyer [16]. However their work considers only stationary noise sources, which is a serious limitation.

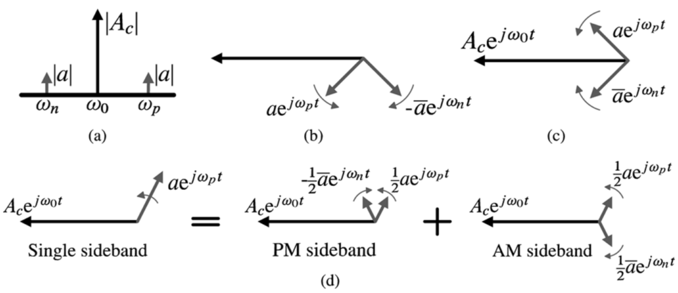

Fig. 2. (a) Sideband magnitudes do not reveal modulation type. (b) PM sidebands: sum is orthogonal to carrier. (c) AM sidebands: sum is colinear with carrier. (d) A single sideband around can be decomposed into equal PM and AM sidebands.

where $G_M[k]$ describes the Fourier series coefficients of the instantaneous conductance, $G_m(t)$.[4] As per (3), sustained oscillations mandate that $\langle P_{\mathrm{TANK}}\rangle + \langle P_{\mathrm{NR}}\rangle = 0$. Combining this requirement with (8), and noting that $\langle P_{\mathrm{TANK}}\rangle = A_c^2/(2R_p)$ leads to the identity

$$G_{M_{\mathrm{EFF}}} = G_M[0] - G_M[2] = -\frac{1}{R_p} \tag{9}$$

which is the effective conductance derived by Samori *et al.* [7]. The mixing action of the ideal sinusoidal output with the time-varying conductance ensures that only components at dc and the second harmonic ultimately contribute to $G_{M_{\mathrm{EFF}}}$. This energy-conservation requirement (i.e., power dissipated in the tank is equal to power returned by the nonlinearity), is central to our rederivation of the Bank's general result. It is interesting to note the similarity between the $G_{M_{\mathrm{EFF}}}$ of the time-varying conductance derived above and the C_{EFF} of the time-varying capacitance derived in [20].

III. "Noiseless" Oscillator Injected With a Small Current Source

We now analyze the effect of a small external current injected differentially into a "noiseless" negative-gm oscillator. We assume that noise does not shift the average frequency of oscillation but merely spreads the spectrum across symmetrical noise sidebands. This analysis leads to transfer functions that maps a small differentially-referred current source to the oscillator's output.

A. Recognizing Phase and Amplitude Modulating Sidebands

Consider a pair of sidebands around a large carrier, as in Fig. 2(a). Assume the magnitudes of the sidebands are equal and small with respect to the carrier. If the relative phases of the sidebands are such that their sum is orthogonal at all times with the carrier, phase modulation results. This modulation is shown in the phasor plot, Fig. 2(b). Alternatively, if the sum is always colinear to the carrier, amplitude modulation results, as shown in Fig. 2(c). A single-sideband around a carrier can always be decomposed into equal PM and AM sidebands as shown in Fig. 2(d) [21].

[4]This work uses the complex exponential form of the Fourier series that defines the coefficients in terms of the double-sided frequency spectrum, i.e., $x(t) = \sum_{k=-\infty}^{\infty} X[k]\mathrm{e}^{jk\omega_0 t}$.

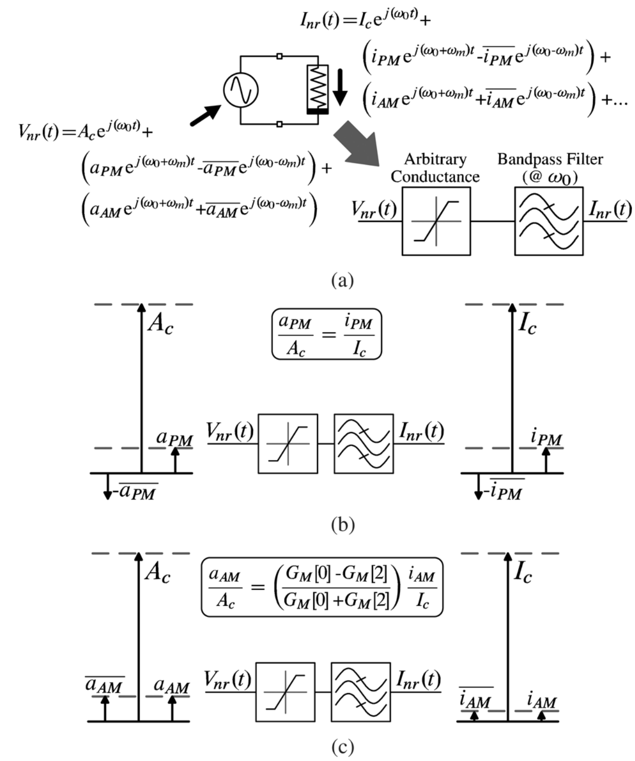

Fig. 3. Response of the nonlinearity to an AM and PM signal. (a) Nonlinearity modeled as a memoryless conductance followed by a bandpass filter. (b) Response of the band-limited nonlinearity to phase modulated carrier. (c) Response of the band-limited nonlinearity to amplitude modulated carrier.

B. Response of the Nonlinearity to AM/PM Modulated Carriers

To properly quantify noise in the negative-gm model, a correct understanding of the response of the nonlinearity to both AM and PM modulated carriers is required. The most general explanation we have encountered is that presented by Samori *et al.* [7].[5] Essentially, Samori *et al.* model the nonlinearity as an arbitrary nonlinear conductance followed by a bandpass filter, as shown in Fig. 3(a). The bandpass filter, which is simply the oscillator's tank, suppresses terms that do not lie close to the carrier frequency.

Using this approach, Samori *et al.* demonstrate that, in the case of a phase modulated signal, the sideband-to-carrier ratio at the input is identical to the sideband-to-carrier ratio at the output, i.e.,

$$\frac{i_{\mathrm{PM}}}{I_c} = \frac{a_{\mathrm{PM}}}{A_c}. \tag{10}$$

The above expression differs in notation from Samori *et al.*; a complete proof and discussion of the above expression is given in [17]. Extending this analysis to the case of an AM signal, Samori *et al.* show that the sideband-to-carrier ratio at the input is related to the sideband-to-carrier ratio at the output as follows:

$$\frac{i_{\mathrm{AM}}}{I_c} = \left(\frac{G_M[0] + G_M[2]}{G_M[0] - G_M[2]}\right)\frac{a_{\mathrm{AM}}}{A_c}. \tag{11}$$

[5]The narrowband response of a nonlinearity to a noisy signal has been investigated by many others (see discussion in [17]). Indeed, using an analysis method developed for mixers [22], we previously quantified such a response for the specific case of the current-biased topology [9].

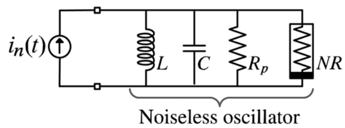

Fig. 4. Noiseless negative-gm oscillator excited by an external current source.

The response of the nonlinearity to a PM carrier is visualized in Fig. 3(b), while the nonlinearity's response to an AM carrier is visualized in Fig. 3(c).

C. Response of the Negative-gm Oscillator to an External Current Source

Consider a current source, i_n, in parallel with a noiseless negative-gm oscillator, as shown in Fig. 4. Assume the circuit supports a sustained oscillation and the current source has two frequency components at $\omega_0 \pm \omega_m$. As shown in the previous section, the nonlinearity can be viewed as a voltage-to-current transfer function that preserves the frequency and phase (but not the magnitude) of a carrier and any sidebands, and does not produce frequency components with significant amplitudes at other frequencies.[6] This simplification coupled with the assumption of a linear tank, ensures that the output of the oscillator is of the form

$$\begin{aligned} V_{\text{out}}(t) = A_c \mathrm{e}^{j\omega_0 t} &+ \left(a_{\text{PM}} \mathrm{e}^{j\omega_p t} - \overline{a_{\text{PM}}} \mathrm{e}^{j\omega_n t}\right) \\ &+ \left(a_{\text{AM}} \mathrm{e}^{j\omega_p t} + \overline{a_{\text{AM}}} \mathrm{e}^{j\omega_n t}\right) \end{aligned} \tag{12}$$

where $\overline{a}$ denotes the conjugate of complex number a, $\omega_p = \omega_0 + \omega_m$, $\omega_n = \omega_0 - \omega_m$, a_{PM} is the PM sideband component, and a_{AM} is the AM sideband component. This output waveform excites the following current from the nonlinearity

$$\begin{aligned} I_{\text{nr}}(t) &= I_c \mathrm{e}^{j\omega_0 t} + \left(i_{\text{PM}} \mathrm{e}^{j\omega_p t} - \overline{i_{\text{PM}}} \mathrm{e}^{j\omega_n t}\right) \\ &\quad + \left(i_{\text{AM}} \mathrm{e}^{j\omega_p t} + \overline{i_{\text{AM}}} \mathrm{e}^{j\omega_n t}\right) \\ &= -\frac{A_c}{R_p} \mathrm{e}^{j\omega_0 t} - \frac{1}{R_p}\left(a_{\text{PM}} \mathrm{e}^{j\omega_p t} - \overline{a_{\text{PM}}} \mathrm{e}^{j\omega_n t}\right) \\ &\quad + \left(G_M[0] + G_M[2]\right)\left(a_{\text{AM}} \mathrm{e}^{j\omega_p t} + \overline{a_{\text{AM}}} \mathrm{e}^{j\omega_n t}\right). \end{aligned} \tag{13}$$

Applying KCL to the oscillator in Fig. 4, we can extract an expression for the phasor V_{out}, in terms of the injected noise current and the nonlinearity current

$$V_{\text{out}}(s) = -\frac{(-i_n(s) + I_{\text{NR}}(s)) sLR_p}{R_p + sL + s^2 LR_p C}. \tag{14}$$

The Laplace transform is valid because we are relating the voltage and current by means of a linear tank. Assuming $s = j(\omega_0 \pm \omega_m)$ and $\omega_m \ll \omega_0$

$$\begin{aligned} &V_{\text{out}}\{\omega_0 \pm \omega_m\} \approx \\ &\qquad \frac{j(-i_n\{\omega_0 \pm \omega_m\} + I_{\text{NR}}\{\omega_0 \pm \omega_m\})\omega_0 LR_p}{-j\omega_0 L \pm 2R_p\left(\frac{\omega_m}{\omega_0}\right)}. \end{aligned} \tag{15}$$

We can view the injected current source, i_n, as a signal that modulates the amplitude and/or phase of the fundamental of the current from the nonlinear resistor, I_c. In order to modulate the phase of I_c, the injected current needs to be of the form: $i_n(t) = (i_x/2)\mathrm{e}^{j(\omega_0+\omega_m)t} - (\overline{i_x}/2)\mathrm{e}^{j(\omega_0-\omega_m)t}$. Using (12), (13), and (15) and solving for specific frequencies results in

$$\begin{aligned} &a_{\text{PM}} + a_{\text{AM}} \\ &\quad = \frac{j\left(-\frac{i_x}{2} - \frac{a_{\text{PM}}}{R_p} + \left(2G_M[0] + \frac{1}{R_p}\right)a_{\text{AM}}\right)\omega_0 LR_p}{-j\omega_0 L + R_p\left(2\frac{\omega_m}{\omega_0}\right)} \\ &-\overline{a_{\text{PM}}} + \overline{a_{\text{AM}}} \\ &\quad = \frac{j\left(\frac{\overline{i_x}}{2} + \frac{\overline{a_{\text{PM}}}}{R_p} + \left(2G_M[0] + \frac{1}{R_p}\right)\overline{a_{\text{AM}}}\right)\omega_0 LR_p}{-j\omega_0 L - R_p\left(2\frac{\omega_m}{\omega_0}\right)}. \end{aligned} \tag{16}$$

Solving for a_{PM} and a_{AM} gives

$$\begin{aligned} a_{\text{PM}} &= -j\frac{(i_x/2)\omega_0^2 L}{2\omega_m} \\ &= (i_x/2) Z_{\text{PM}}\{\omega_0 + \omega_m\} \\ a_{\text{AM}} &= 0 \end{aligned} \tag{17}$$

where $Z_{\text{PM}}\{\omega_0 + \omega_m\}$ is the impedance of the *lossless* tank. Therefore, a current source in parallel with the tank that modulates the phase of I_c will flow through an impedance defined by the lossless tank. In doing so, it will generate PM sidebands around the output carrier. External current of this form cannot cause AM sidebands. The impedance seen by this "phase modulating" injected current is shown in Fig. 5(a).

Similarly, it can be shown that a current source that modulates the amplitude of I_c (i.e., $i_n(t) = (i_x)/(2)\mathrm{e}^{j(\omega_0+\omega_m)t} + (\overline{i_x})/(2)\mathrm{e}^{j(\omega_0-\omega_m)t}$), will generate the following sideband components:

$$\begin{aligned} a_{\text{PM}} &= 0 \\ a_{\text{AM}} &= \frac{i_x/2}{\left(G_M[0] + G_M[2] + \frac{1}{R_p}\right) - \frac{2\omega_m}{j\omega_0^2 L}}. \end{aligned} \tag{18}$$

Thus an "amplitude modulating" injected current will see the impedance shown in Fig. 5(b). External current of this form will generate AM sidebands only. In the extreme case of a linear oscillator (i.e., the conductance of the energy-restoring mechanism is linear, $G_M[0] \approx -1/R_p$ and $G_M[2] \approx 0$) amplitude noise will flow into the lossless tank and produce sidebands equal in magnitude to that produced by an equivalent PM current source. While a truly linear oscillator is unrealizable, it can be approximated using automatic gain control (as discussed in [16]). However, in more conventional circuits, AM sidebands at close-in offsets are generally negligible compared to PM sidebands.

While the calculations presented so far are somewhat tedious, the results are remarkably simple and shown as follows.

- An injected current that modulates the phase of the fundamental of the nonlinearity current will be shaped by the impedance of the *lossless* tank and generate PM sidebands around the output carrier.
- An injected current that modulates the amplitude of the fundamental of the nonlinearity current will be shaped by

[6] Since the conductance is, in general, strongly nonlinear, current components of significant magnitudes are generated at frequencies other than the fundamental. These components, however, are far from the oscillation frequency and are greatly attenuated by the tank.

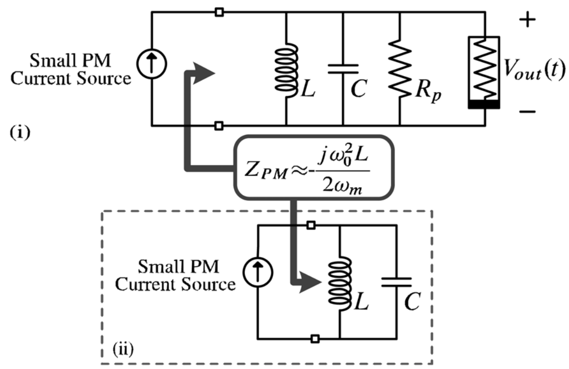

(a)

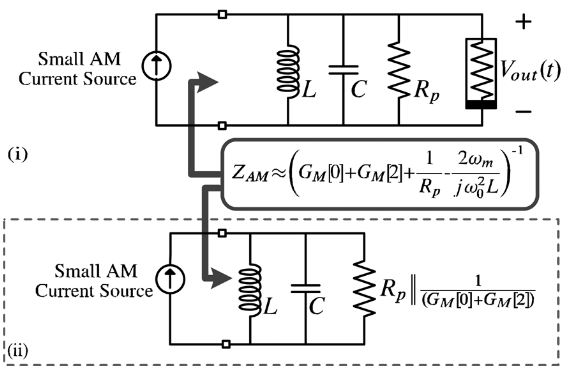

(b)

Fig. 5. Differential current source acting on a "noiseless" oscillator. (a) Phase modulating case: (i) PM current injected into oscillator; (ii) Impedance seen by PM current source. (b) Amplitude modulating case: (i) AM current injected into oscillator; (ii) Impedance seen by AM current source.

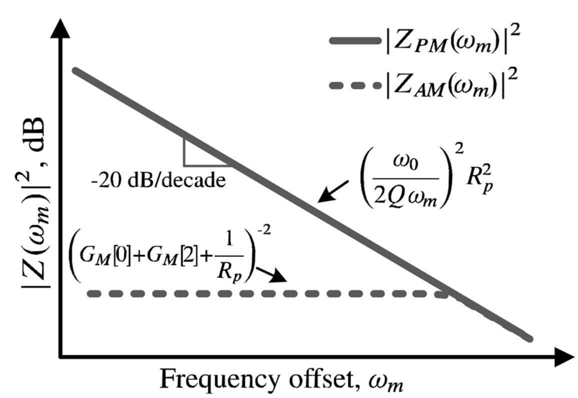

Fig. 6. Squared impedance seen by phase and amplitude modulating currents.

the *lossy* resonator of Fig. 5(b) and generate AM sidebands around the output carrier.

The squared impedances "seen" by phase and amplitude modulating currents are plotted in Fig. 6, and given by

$$\boxed{|Z_{\mathrm{PM}}\{\omega_0 \pm \omega_m\}|^2 = \left(\frac{\omega_0^4 L^2}{4\omega_m^2}\right) = \left(\frac{\omega_0}{2Q\omega_m}\right)^2 R_p^2} \tag{19}$$

$$\boxed{|Z_{\mathrm{AM}}\{\omega_0 \pm \omega_m\}|^2 = \frac{1}{\left(G_M[0]+G_M[2]+\frac{1}{R_p}\right)^2+\left(\frac{2\omega_m}{\omega_0^2 L}\right)^2},} \tag{20}$$

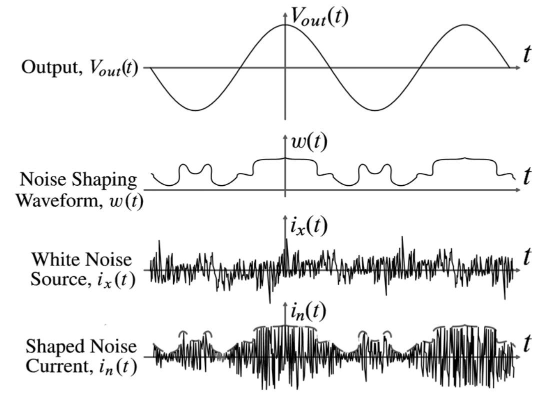

Fig. 7. Cyclostationary white noise modeled as a white noise source modulated by a periodic waveform.

where $G_M[k]$ is calculated with respect to a zero-initial-phase cosine output voltage. Since we will ultimately deal with current noise, the above equations can be viewed as transfer functions that map the AM and PM components of resonator-referred differential noise current to output noise.

Our analysis can be viewed as an extension of the work of Samori *et al.* [7] and Kouznetsov and Meyer [16]. The approach is similar in spirit to that presented by Samori *et al.* [7], although he did not frame the theory in terms of generalized transfer functions; Kouznetsov and Meyer [16] derived a transfer function that maps a stationary current noise to output noise, but did not consider correlated sidebands (i.e., AM/PM sidebands).

The exact approach, however, is a generalized version of that we have previously laid out in [17], which was itself a refinement of [9]. Indeed, in the limiting case of a "hard-switching" linearity, the above analysis degenerates into what we have presented in [9].[7]

IV. Decomposition of a Resonator-Referred Cyclostationary White Noise Source

In the previous section, we derived transfer functions (19) and (20) that facilitate the mapping of small AM and PM current sources (referred across the tank) to the oscillator's output. In this section, we show how to a decompose an arbitrary cyclostationary white noise source [18] into its AM and PM components. These AM/PM components can then be applied directly to (19) and (20).

Consider again the noiseless oscillator shown in Fig. 4. In this instance, assume that the external current source, i_n, is a noise source that is cyclostationary at the oscillation frequency. We can model this current source as a stationary white noise source, i_x, modulated by an arbitrary periodic real-valued waveform, $w(t)$ [18]. Accordingly, i_n will have a time-varying power spectral density equal to

$$\widehat{i_n^2} = \widehat{i_x^2} w^2(t). \tag{21}$$

The modulation of $i_x(t)$ and $w(t)$ is shown in Fig. 7. The Fourier coefficients of the ω_0-periodic signal $w(t)$ are shown in Fig. 8. The cyclostationary spectrum is found by first modelling white noise as an infinite number of sinusoids separated in frequency

[7] [9] was based on previous work on mixers [22] and used ABCD parameters to deal with carrier sidebands. In [17], the approach was simplified by adopting complex phasor notation, and further refined using results from [23] and Samori *et al.* [7].

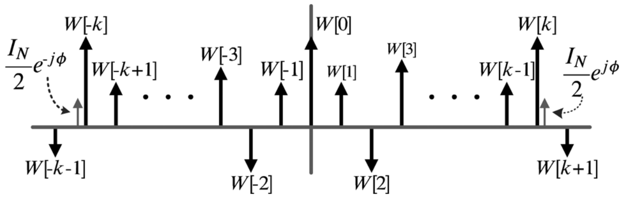

Fig. 8. Frequency spectrum of arbitrary waveform $w(t)$.

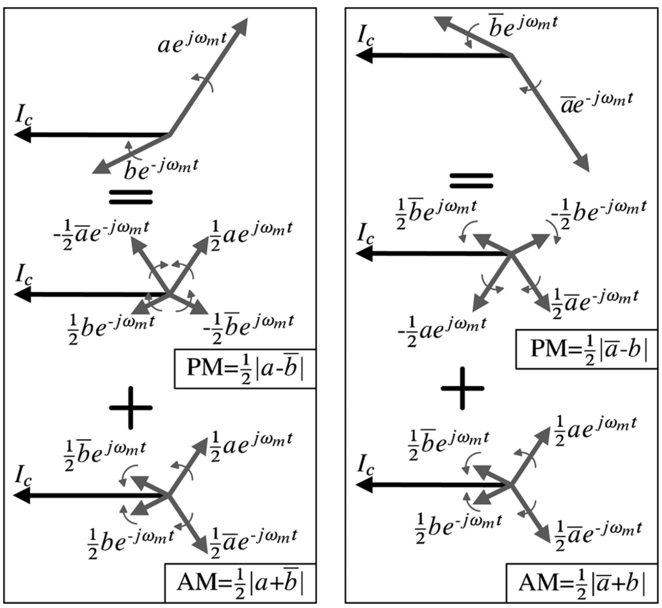

(a) (b)

Fig. 9. Phasor diagrams. (a) Positive frequencies ($e^{j\omega_o t}$ component of each phasor is not shown, but is assumed). (b) Negative frequencies ($e^{-j\omega_o t}$ component of each phasor is not shown, but is assumed).

by 1 Hz and uncorrelated in phase [21]. Consider one such sinusoid located close to kth harmonic of the periodic modulation waveform (see Fig. 8)

$$\begin{aligned} i_{n_k}(t) &= I_N \cos((k\omega_0 + \omega_m)t + \phi) \\ &= \frac{I_N}{2} e^{j\phi} e^{j(k\omega_0+\omega_m)t} \\ &\quad + \frac{I_N}{2} e^{-j\phi} e^{-j(k\omega_0+\omega_m)t} \end{aligned} \tag{22}$$

where and I_N is an arbitrary constant, and ϕ is an arbitrary phase. Mixing $i_{n_k}(t)$ with the waveform $w(t)$ results in the following components around the fundamental:

$$\left.\begin{array}{ll} @\,\omega_0+\omega_m & : a = W[-k+1]\frac{I_N}{2}e^{j\phi} \\ @\,\omega_0-\omega_m & : b = W[k+1]\frac{I_N}{2}e^{-j\phi} \end{array}\right\} \text{ pos freqs.}$$
$$\left.\begin{array}{ll} @\,-\omega_0+\omega_m & : \overline{b} = W[-k-1]\frac{I_N}{2}e^{j\phi} \\ @\,-\omega_0-\omega_m & : \overline{a} = W[k-1]\frac{I_N}{2}e^{-j\phi} \end{array}\right\} \text{ neg freqs.} \tag{23}$$

The output voltage, $V_{\rm out}(t) = A_c \cos(\omega_0 t)$ excites a current from the nonlinearity whose fundamental component is $I_c(t) = -(A_c/R_p)\cos(\omega_0 t)$. Knowing this, we can construct the phasor diagrams shown in Fig. 9, which enables us to decompose the resulting sidebands into AM and PM sidebands. As a result of i_{n_k}, the total power[8] of the phase modulating sidebands around the fundamental is calculated as

$$\mathcal{S}_{\rm PM}(k) = \frac{1}{4}(|a-\overline{b}|^2 + |\overline{a}-b|^2) = \frac{1}{2}(|a-\overline{b}|^2). \tag{24}$$

Substituting the values for a and $\overline{b}$ from (23) gives

$$\mathcal{S}_{\rm PM}(k) = \left(\frac{I_N^2}{8}\right)|W[-k+1] - W[-k-1]|^2. \tag{25}$$

Summing k from $-\infty$ to ∞ accounts for noise around all harmonics at both $k\omega_0 - \omega_m$ and $k\omega_0 + \omega_m$

$$\begin{aligned} \mathcal{S}_{\rm PM_{TOT}} &= \sum_{k=-\infty}^{\infty} \mathcal{S}_{\rm PM}(k) \\ &= \left(\frac{I_N^2}{8}\right) \sum_{k=-\infty}^{\infty} (2|W[k]|^2 - W[-k+1]\overline{W[-k-1]} \\ &\quad - W[-k-1]\overline{W[-k+1]}) \\ &= \left(\frac{I_N^2}{8}\right) \sum_{k=-\infty}^{\infty} (2|W[k]|^2 \\ &\quad - W[-k+1]W[k+1] - W[-k-1]W[k-1]). \end{aligned} \tag{26}$$

Substituting $(I_N^2/2) = \widehat{i_x^2}$ into the above expression gives the PSD of the noise current that modulates the phase of the fundamental of the nonlinear current

$$\widehat{i^2_{n_{\rm PM}}} = \frac{\widehat{i_x^2}}{4}\left(\sum_{k=-\infty}^{\infty} 2|W[k]|^2 - \sum_{k=-\infty}^{\infty} W[k]W[2-k] - \sum_{k=-\infty}^{\infty} W[k]W[-2-k]\right). \tag{27}$$

To simplify further, we recognize that

$$p(t) \doteq w(t)w(t) \overset{FS;\omega_0}{\longleftrightarrow} P[k] = \sum_{l=-\infty}^{\infty} W[l]W[k-l] \tag{28}$$

and therefore, we may write $\widehat{i^2_{n_{\rm PM}}}$ as follows:

$$\boxed{\widehat{i^2_{n_{\rm PM}}} = \left(\tfrac{1}{2}P[0] - \tfrac{1}{4}P[2] - \tfrac{1}{4}P[-2]\right)\widehat{i_x^2},} \tag{29}$$

where $P[k]$ is the Fourier series component of the square of the noise shaping function, $w(t)$. Using a similar derivation and employing the same assumptions, it can be shown that the AM component is given by

$$\boxed{\widehat{i^2_{n_{\rm AM}}} = \left(\tfrac{1}{2}P[0] + \tfrac{1}{4}P[2] + \tfrac{1}{4}P[-2]\right)\widehat{i_x^2}.} \tag{30}$$

Thus, if we know the noise shaping waveform (i.e., $w(t)$), we can easily decompose a noise source into its AM/PM components. This decomposition, coupled with the transfer functions described by (19) and (20), allow us to quantify a given source's contribution to output noise.

[8]Defined in terms of the single-sided frequency spectrum.

V. Noise Factor of the Negative-Gm Model

In this section, we use the preceding analysis to derive an expression for noise in the negative-gm oscillator (see Fig. 1). In doing so, we are using our phasor-based approach instead of Bank's ISF analysis to rederive his general result [14], [15]. Our approach also enables us to quantify, for the first time, noise due to amplitude fluctuations.

A. Noise From Resonator Losses

Decomposing the noise associated with the tank resistance, R_p, is a trivial case of the noise analysis presented in the previous section; the noise current, $\widehat{i^2_{\rm res}} = 4kT/R_p$, is simply a white noise source, modulated by the constant window $w(t) = 1$. Accordingly,

$$p(t) = w(t)w(t) = 1 \overset{FS;\omega_0}{\longleftrightarrow} P[k] = \delta[k]. \tag{31}$$

Therefore

$$\widehat{i^2_{{\rm res}_{\rm PM}}} = \widehat{i^2_{{\rm res}_{\rm AM}}} = \frac{2kT}{R_p} \tag{32}$$

which is half the total resistor current noise.

B. Noise From the Nonlinearity

The noise from the nonlinearity is modeled as a cyclostationary white noise current source, $i_{\rm nr}$, in parallel with the tank. We assume, further, that the time-varying PSD of this current source is proportional to the instantaneous conductance of the nonlinearity itself,[9] i.e.,

$$\widehat{i^2_{\rm nr}} = -\widehat{i^2_x} G_m(t) \tag{33}$$

where

$$\widehat{i^2_x} = 4kT\alpha \tag{34}$$

is an arbitrary stationary white noise source, α is an arbitrary noise intensity constant, and $G_m(t)$ is the instantaneous conductance. Accordingly, the noise current, $i_{\rm nr}$, is simply the white noise source, i_x, modulated by the window $w(t) = \sqrt{-G_m(t)}$. In general, a memoryless nonlinearity excited by a zero-initial-phase cosine wave will generate a $G_m(t)$ waveform that is a real and even function of time. We further assume that $G_m(t) \leq 0$ at all times.[10] Therefore

$$p(t) = w(t)w(t) = \sqrt{-G_m(t)}\sqrt{-G_m(t)} = -G_m(t) \tag{35}$$

and thus we can deduce from (29) and (30) that

$$\begin{aligned} \widehat{i^2_{{\rm nr}_{\rm PM}}} &= -\frac{1}{2}(G_M[0] - G_M[2])\widehat{i^2_x} \\ \widehat{i^2_{{\rm nr}_{\rm AM}}} &= -\frac{1}{2}(G_M[0] + G_M[2])\widehat{i^2_x} \end{aligned} \tag{36}$$

since $G_M[2] = G_m[-2]$. Recognizing that the PM component is directly proportional to the effective conductance of the nonlinearity defined in (9) we write

$$\widehat{i^2_{{\rm nr}_{\rm PM}}} = \frac{\widehat{i^2_x}}{2R_p} = \frac{2kT\alpha}{R_p}. \tag{37}$$

Amazingly, given the above assumptions, the component of $i_{\rm nr}$ that is responsible for phase modulation of the carrier current (and thus phase noise) is completely *independent* of the shape of the nonlinear characteristic. Put another way: a hard-limiting and soft-limiting nonlinearity will inject exactly the same PM noise into the oscillator.

C. General Result and Implications

The phase modulating components of the resistor and nonlinearity noise will be shaped by (19), while the amplitude modulating components will be shaped by (20). Thus the output voltage noise that causes phase fluctuations is

$$\widehat{v^2_{n_{\rm PM}}} = \left(\widehat{i^2_{{\rm res}_{\rm PM}}} + \widehat{i^2_{{\rm nr}_{\rm PM}}}\right)|Z_{\rm PM}\{\omega_0 \pm \omega_m\}|^2 \tag{38}$$

which evaluates to

$$\boxed{\widehat{v^2_{n_{\rm PM}}} = 2kT(1+\alpha)R_p\left(\frac{\omega_0}{2Q\omega_m}\right)^2.} \tag{39}$$

Equating this expression with (1), we see that the noise factor depends only on the noise intensity constant α and is given by

$$\boxed{F = 1 + \alpha.} \tag{40}$$

Equivalently, the output noise due to amplitude fluctuations is

$$\widehat{v^2_{n_{\rm AM}}} = \left(\widehat{i^2_{{\rm res}_{\rm AM}}} + \widehat{i^2_{{\rm nr}_{\rm AM}}}\right)|Z_{\rm AM}(\omega_0 \pm \omega_m)|^2 \tag{41}$$

which evaluates to

$$\boxed{\widehat{v^2_{n_{\rm AM}}} = \frac{2kT/R_p - 2kT\alpha(G_M[0]+G_M[2])}{\left(G_M[0]+G_M[2]+\frac{1}{R_p}\right)^2 + \left(\frac{2\omega_m}{\omega_0^2 L}\right)^2}} \tag{42}$$

where $G_M[k]$ is calculated with respect to a zero-initial-phase cosine output voltage. As stated before, $\widehat{v^2_{n_{\rm AM}}} \ll \widehat{v^2_{n_{\rm PM}}}$ at close-in offsets and can be ignored. Therefore, in a nearly sinusoidal *LC* oscillator, if the energy restoring nonlinearity is memoryless, possesses an instantaneous small-signal conductance that is negative throughout the oscillation, and has a noise current whose PSD is proportional to the instantaneous small-signal conductance, then that oscillator's noise factor will be independent of the nonlinear characteristic.

Although presented in a different form, this is the general result derived by Bank [14] and Andreani and Mazzanti [15].[11] Indeed, there appears to be no quantitative difference between the phasor-based approach and the ISF approach, as it applies

[9]As will be shown in Section VI, this is typically the case for CMOS oscillators when only channel noise is considered. It is also a good approximation for high-beta bipolar oscillators where collector shot noise typically dominates. However, if noise due to gate resistance (in CMOS oscillators) or noise arising from parasitic base resistance (in bipolar oscillators) dominates, the resultant conductance noise will be proportional to $G^2_m(t)$. The latter case is examined in [7].

[10]This is not always the case (see Section VII), and is merely a criterion of the general result.

[11]In [15], the noise factor is presented as $F = 1 + \gamma\eta/\alpha_m$, where γ is an intensity factor, η is a feedback factor, and α_m is a gain factor. By redrawing in the form of the negative-gm model, we do not make these distinctions, and so $\alpha = \gamma\eta/\alpha_m$.

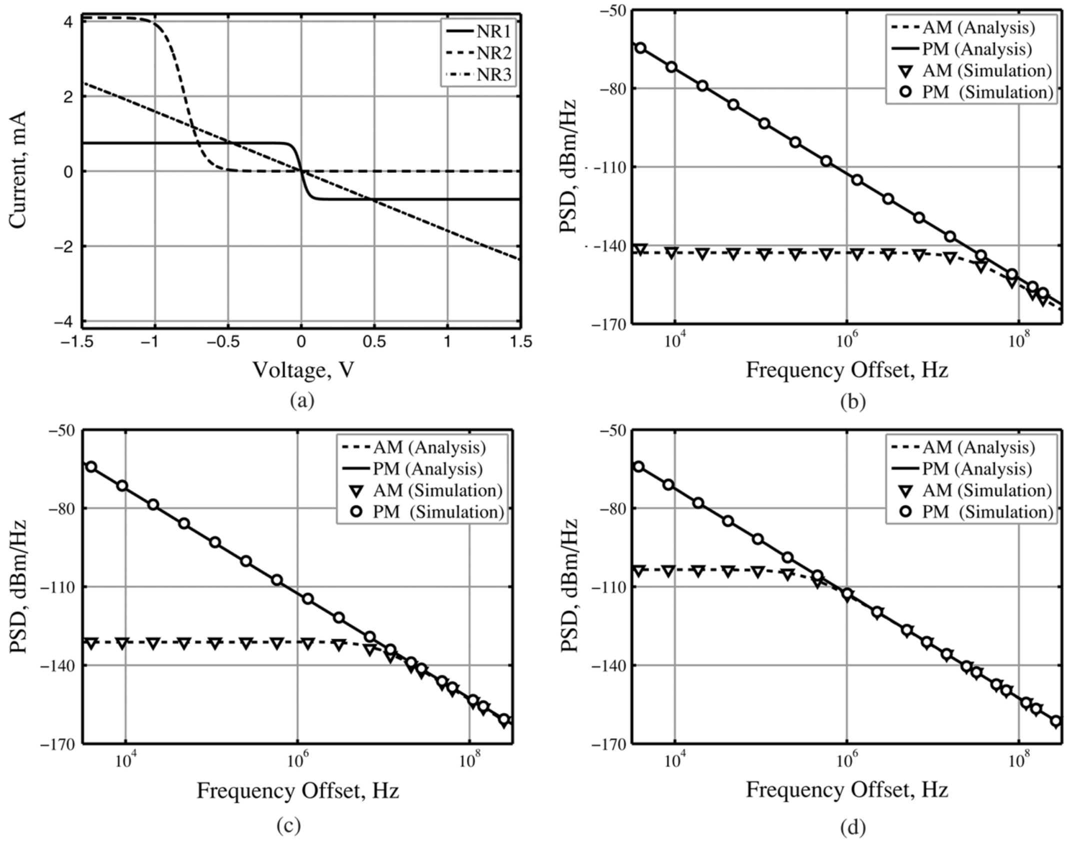

Fig. 10. Generic negative-gm oscillator simulations. (a) Simulated IV characteristics. (b) NR1—AM and PM sidebands. (c) NR2—AM and PM sidebands. (d) NR3 - AM and PM sidebands.

to output noise resulting from phase fluctuations in nearly sinusoidal *LC* oscillators. This is discussed in greater detail in Appendix A. Output noise resulting from amplitude fluctuations has not yet been quantified using the ISF approach.

Many popular CMOS *LC* oscillators—notably the standard current-biased nMOS/CMOS and Colpitts topologies—satisfy Bank's general result, and thus quantifying the output noise of a given oscillator becomes a simple matter of determining the noise intensity constant α.

D. SpectreRF Simulations

The generic negative-gm *LC* oscillator, shown in Fig. 1, was simulated using SpectreRF. The negative-gm resistor was modeled in Verilog-A, and the tank components were chosen as $R_p = 628\ \Omega$, $L = 5$ nH, and $C = 5$ pH. Three different I-V characteristics, shown in Fig. 10(a), were simulated as follows.

- *NR1:* Hard-limiting ($\approx$ standard topology, see Fig. 11).
- *NR2:* Asymmetric [$\approx$ Colpitts topology, see Fig. 13(a)].
- *NR3:* Soft-limiting[12] ($\approx$ linear, or ALC-assisted).

In each case, the associated noise current, $i_{\rm nr}$, had a PSD equal to $-4kT\alpha G_m(t)$, with $\alpha = 2/3$. The predicted and simulated output noise (in dBm/Hz) due to AM and PM for the three oscillators are plotted in Figs. 10(b)–(d). We see the following.

- All nonlinearities lead to the same output noise (in dBm/Hz) due to phase fluctuations.
- The output noise (in dBm/Hz) due to amplitude fluctuations varies considerably depending on the nonlinearity.
- The oscillator employing the linear negative resistance (NR3) exhibits the largest $\widehat{v^2_{n_{\rm AM}}}$ component. Since NR3 possesses a very weak nonlinearity, it struggles to suppress amplitude disturbances; $G_M[0] \approx -1/R_p$ and $G_M[2] \approx 0$.
- The oscillator employing NR1 has a very small $\widehat{v^2_{n_{\rm AM}}}$ component. In this case, $G_M[0] \approx -G_M[2]$, the nonlinearity contributes no AM noise current, and the AM noise current due to the resistor flows into the lossy resonator only.

The choice of nonlinearity (e.g., hard-limiting or soft-limiting) has no effect on output noise resulting from phase fluctuations. However, it does make a difference to output noise arising from amplitude fluctuations, oscillation amplitude for a given current, and potentially other attributes such as frequency stability and harmonic content [9].

All these observations relate to absolute noise (dBm/Hz) but not relative phase noise normalized to the oscillation amplitude (dBc/Hz); oscillation amplitude depends on the I-V characteristic, and will affect the phase noise measurement when quoted in dBc/Hz.[13]

[12]The characteristic is a piecewise approximation of a linear resistance. Convergence issues set the limit as to how much the characteristic deviates from a straight line.

[13]It can be shown that, for a given power budget, the largest oscillation amplitude will be attained if the restoring current is injected as an impulse at the peak (or trough) of an oscillation [24]. Mazzanti and Andreani [25] made use of this fact to develop a topology, which, from a theoretical viewpoint at least, promises better phase noise performance, for a given current, than any other nMOS-only topology currently conceived. The improved phase noise performance of the topologies proposed by Shekhar *et al.* [26], and Soltanian and Kinget [27] can also be attributed to this fact.

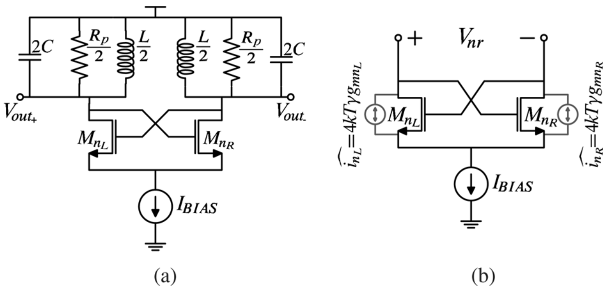

Fig. 11. Standard current-biased nMOS *LC* oscillator. (a) Schematic. (b) Nonlinear negative resistance.

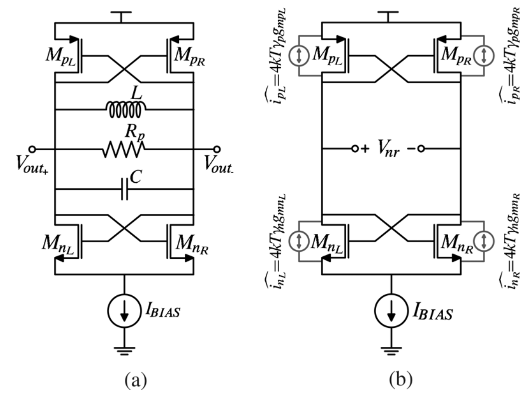

Fig. 12. Standard current-biased CMOS *LC* oscillator. (a) Schematic. (b) Nonlinear negative resistance.

VI. Applying the General Result to Popular Oscillators

The noise factors derived in this section are already known. Rael [9] derived the noise factor for the current-biased nMOS standard topology under hard-switching conditions. Later, Andreani *et al.*, using the ISF, derived the same noise factor but under more general conditions [10], as well as the noise factors for the Colpitts topology [10] and current-biased CMOS standard topology [11]. Our intent is simply to show how the general result, and specifically our interpretation of it, can be applied to these oscillators.

A. Noise Factor

1) The Standard Current-Biased nMOS Topology: The standard nMOS *LC* topology is shown in Fig. 11(a). The energy-restoring nonlinearity is composed of a cross-coupled differential nMOS pair, displayed separately in Fig. 11(b). Assuming an ideal noiseless current source, it is straightforward (see Appendix B) to show that the conductance of the differential pair as a function of time is given by

$$G_m(t) = -\frac{g_{mn_R}(t)g_{mn_L}(t)}{g_{mn_R}(t)+g_{mn_L}(t)} \tag{43}$$

where $g_{mn_R}(t)$ and $g_{mn_L}(t)$ are the instantaneous transconductance of the transistors M_{n_R} and M_{n_L}, respectively. Additionally, as shown in Appendix B, the noise current noise associated with the nonlinearity, i_{nr}, has a time varying power spectral density equal to

$$\widehat{i^2_{\mathrm{nr}}} = -4kT\gamma G_m(t) \tag{44}$$

where γ is the channel noise coefficient of an nMOS transistor. As per (33), the noise associated with the differential pair is proportional to its conductance, which is memoryless and always negative. Therefore, the general result applies, and by mere inspection we see that the noise intensity constant, α, in (39) is equal to γ. Thus, the output power spectral density of the oscillator is equal to

$$\widehat{v^2_n} = 2kTR_p\,(1+\gamma)\left(\frac{\omega_0}{2Q\omega_m}\right)^2. \tag{45}$$

Comparing this expression with (2), the minimum possible noise factor of this topology evaluates to

$$\boxed{F_{\mathrm{nMOS}_{\mathrm{MIN}}} = 1+\gamma.} \tag{46}$$

What is remarkable about the above derivation is how little we know about the differential pair. We have said nothing about the size of the transistors, technology or biasing. In fact, we haven't even remarked about matching between the two transistors; the general result suggests that a badly matched pair will have exactly the same output noise as a perfectly matched differential pair![14] The amplitude of oscillation is also irrelevant, as the noise factor remains constant whether the differential pair is hard-switched or not (as stated but not shown in [10]).

2) Standard Current-Biased CMOS Topology: A full CMOS implementation of the standard current-biased topology is shown in Fig. 12(a). The addition of cross-coupled pMOS transistors facilitates the commutation of the bias current across the entire tank (not just half); this doubles the oscillation amplitude for a given current and results in increased oscillator efficiency. Assuming a nearly-sinusoidal oscillation, the negative resistance shown in in Fig. 12(b), will have a time-varying conductance of

$$G_m(t) = -\frac{g_{mn_R}(t)g_{mn_L}(t)}{g_{mn_R}(t)+g_{mn_L}(t)} - \frac{g_{mp_R}(t)g_{mp_L}(t)}{g_{mp_R}(t)+g_{mp_L}(t)} \tag{47}$$

where g_{mn_R}, g_{mn_L}, g_{mp_R}, and g_{mp_L} are the transconductances of M_{n_R}, M_{n_L}, M_{p_R}, and M_{p_L}, respectively. It can be shown that this topology injects a noise current, i_{nr}, into the tank whose PSD is

$$\widehat{i^2_{\mathrm{nr}}} = 4kT\left(\gamma_n\frac{g_{mn_R}(t)g_{mn_L}(t)}{g_{mn_R}(t)+g_{mn_L}(t)} + \gamma_p\frac{g_{mp_R}(t)g_{mp_L}(t)}{g_{mp_R}(t)+g_{mp_L}(t)}\right). \tag{48}$$

Assuming $\gamma \approx \gamma_n \approx \gamma_p$

$$\widehat{i^2_{\mathrm{nr}}} = -4kT\gamma G_m(t). \tag{49}$$

[14] We have verified this in simulation.

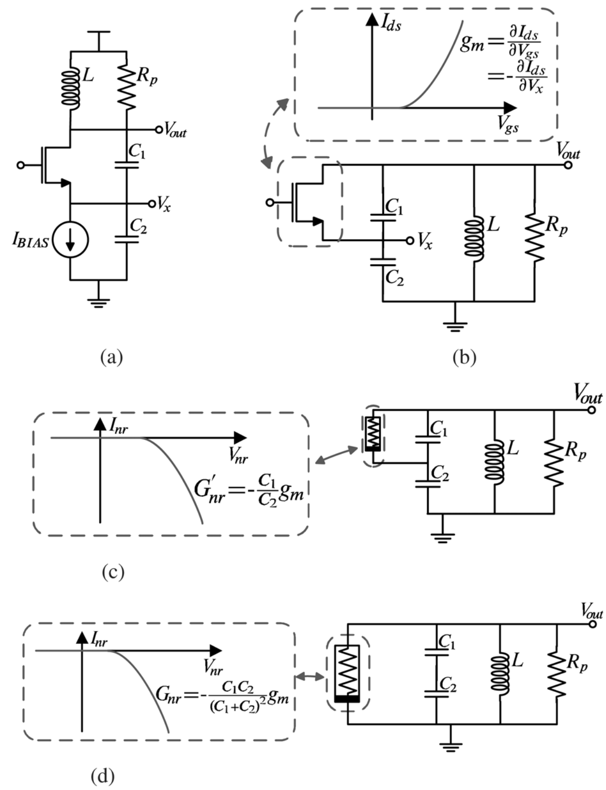

Fig. 13. Colpitts oscillator. (a) Schematic. (b) Simplified schematic—biasing information ignored. (c) Simplified schematic—conducting transistor modeled as a nonlinear negative resistor. (d) Simplified schematic—negative-gm equivalent.

Again, by inspection we see that the noise intensity constant α is equal to γ. Thus, from our analysis above the oscillator's output PSD is given by

$$\widehat{v_n^2} = 2kTR_p(1+\gamma)\left(\frac{\omega_0}{2Q\omega_m}\right)^2 \tag{50}$$

with the minimum noise factor again evaluating to

$$\boxed{F_{\text{CMOS}_{\text{MIN}}} = 1+\gamma.} \tag{51}$$

This is identical to the noise factor of the nMOS only topology;[15] the pMOS transistors double the oscillation amplitude without introducing extra noise into the system. This result was derived previously under the assumption of hard-switching [11].

However, and this is of practical importance, it was noted in [11] that this noise factor can only be obtained if the tank capacitance appears only *between the output terminals*. Capacitance, parasitic or otherwise, from the output terminals to ground offers a path for high frequency noise in the pMOS devices and this can degrade the phase noise factor significantly.

3) Colpitts Topology: The Colpitts oscillator, shown in Fig. 13(a), can be analyzed in a similar fashion. To facilitate such analysis it is first necessary to redraw the circuit in the form of a negative-gm oscillator. It is assumed that, at the oscillation frequency and above, the transistor is not loaded by the capacitors, i.e., at ω_0 the capacitors act as a perfect voltage divider, $g_m \ll \omega_0(C_1+C_2)$ and $V_x \approx V_{\text{out}}(C_1/(C_1+C_2))$. Under this assumption, redrawing the circuit becomes a straightforward task, as shown in Fig. 13. Again, we assume the current source is ideal and noiseless. The conductance of the nonlinearity in the redrawn circuit is

$$G_{\text{nr}}(t) = -\frac{C_1C_2}{(C_1+C_2)^2}g_m(t). \tag{52}$$

Assuming the transistor is either off or operates in the saturation region, noise current, i_n between its drain and source has a time-varying PSD given by $4kT\gamma g_m(t)$. This noise current may be transformed in an identical manner into a differential current across the resonator, and results in a noise current i_{nr} with a power spectral density of

$$\widehat{i_{\text{nr}}^2} = 4kT\gamma\left(\frac{C_2}{C_1+C_2}\right)^2 g_m(t) = -4kT\gamma\left(\frac{C_2}{C_1}\right)G_{\text{nr}}(t). \tag{53}$$

Since the circuit is now in the form of a generalized negative-gm oscillator, we know, by inspection, that $\alpha = \gamma((C_2)/(C_1))$ and thus

$$\widehat{v_n^2} = 2kTR_p\left(1+\gamma\frac{C_2}{C_1}\right)\left(\frac{\omega_0}{2Q\omega_m}\right)^2 \tag{54}$$

and

$$\boxed{F_{\text{Colpitts}_{\text{MIN}}} = 1+\tfrac{C_2}{C_1}\gamma.} \tag{55}$$

Again, it is remarkable that we are able to predict phase noise with almost no information about the specifics of the transistor and its biasing. Does I_{ds} relate to V_x by means of a linear, cubic or higher order polynomial? For what value of V_x does the transistor switch on? To the first order, it doesn't matter. Most notably, the above calculations demonstrate that output noise is independent of the conduction angle. The original derivation [10] is accompanied with a useful discussion on why this topology is inferior to the standard *LC*.

B. Extrinsic Noise

So far we have not addressed noise associated with the bias currents. Again, the effects of these sources are well-known, and are easily accounted for using our technique. Consider first the current-biased nMOS topology with a MOS current source: if the differential pair is hard-switched the current source noise, $\widehat{i_{cs}^2} = 4kT\gamma g_{m_{cs}}$, will be modulated by a square wave of amplitude $\pm(1/2)$, and injected across the tank. Therefore $p(t)$ will be a constant of value $(1/4)$ and $P[k]$ will evaluate to $\delta[k]/4$. This gives

$$\begin{aligned}\widehat{i_{cs_{\text{PM}}}^2} &= \left(\frac{1}{2}P[0]-\frac{1}{4}P[2]-\frac{1}{4}P[-2]\right)\widehat{i_{cs}^2}\\ &= \frac{\widehat{i_{cs}^2}}{8} = \frac{kT\gamma g_{m_{cs}}}{2}\\ \widehat{i_{cs_{\text{AM}}}^2} &= \left(\frac{1}{2}P[0]+\frac{1}{4}P[2]+\frac{1}{4}P[-2]\right)\widehat{i_{cs}^2}\\ &= \frac{\widehat{i_{cs}^2}}{8} = \frac{kT\gamma g_{m_{cs}}}{2}\end{aligned} \tag{56}$$

[15]If $\gamma_n \neq \gamma_p$, the general result does not apply; the calculation of F is significantly complicated, and becomes a function of amplitude and transistor sizing. As shown in [11], however, if the circuit is hard-switched, $F \approx 1+(\gamma_n+\gamma_p)/2$ is a good approximation when $\gamma_n \neq \gamma_p$.

resulting in a noise factor (including all intrinsic sources) of

$$\boxed{F_{\mathrm{nMOS}} = 1 + \gamma + \tfrac{\gamma g_{m_{cs}} R_p}{4}.} \tag{57}$$

Similarly, the noise factor of the CMOS topology becomes

$$\boxed{F_{\mathrm{CMOS}} = 1 + \gamma + \gamma g_{m_{cs}} R_p.} \tag{58}$$

The noise associated with the biasing current source in the Colpitts topology is not modulated, and can be simply referred across the tank (using a Norton Equivalent transformation) as a stationary noise source. Including this source the noise factor becomes

$$\boxed{F_{\mathrm{Colpitts}} = 1 + \tfrac{C_2}{C_1}\gamma + \gamma g_{m_{cs}} R_p \left(\tfrac{C_1}{C_1+C_2}\right)^2.} \tag{59}$$

C. Oscillation Amplitude

Phase noise is always quoted in dBc/Hz, which is simply the single-sideband output PSD normalized to the carrier power (2). The amplitudes of above oscillators are well-known, but in the interest of completeness we give expressions for them. Under hard-switching the amplitude of the nMOS/CMOS standard topologies are

$$\begin{aligned} A_{\mathrm{nMOS}} &= \frac{2}{\pi} I_{\mathrm{BIAS}} R_p \\ A_{\mathrm{CMOS}} &= \frac{4}{\pi} I_{\mathrm{BIAS}} R_p \end{aligned} \tag{60}$$

while the amplitude of the Colpitts oscillator [28] (as the conduction angle, θ, tends to zero) is

$$A_{\mathrm{Colpitts}} = 2 I_{\mathrm{BIAS}} R_p \frac{C_2}{C_1 + C_2}. \tag{61}$$

VII. Q Degradation Analysis

There has always been much concern in oscillator design on how the active elements in the circuit may add to the resonator loss, particularly at the extremes of large oscillation waveforms which may push transistors into their triode regions. The term “loaded Q” refers to these hard to quantify effects which may degrade, sometimes substantially, the inherent resonator Q. Here the general result cannot be used because it requires the conductance of the active nonlinearity to be always negative and/or the associated noise to be proportional to its instantaneous conductance. Our analysis, however, can be extended to deal very neatly with many interesting cases that do not fulfill these criteria. In this work, we investigate the standard voltage-biased nMOS *LC* oscillator and also the standard current-biased CMOS oscillator when subjected to tank loading [11]. “Loaded Q” acquires a quantitative meaning.

A. Arbitrary Nonlinearity That Contributes Loss

Let’s consider the negative-gm model when the conductance is not always negative. We redraw the circuit, as shown in

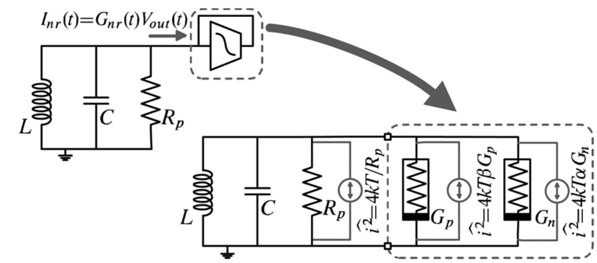

Fig. 14. Generic negative-gm *LC* oscillator model.

Fig. 14, where the nonlinearity is decomposed into two nonlinear resistances: one that is always *positive*, $G_p(t)$, and one that is always *negative*, $G_n(t)$. Further, we assume that we can associate a noise current with each of these resistors that has a PSD proportional to its instantaneous conductance:[16] the noise intensity constants assigned to $G_n(t)$ and $G_p(t)$ are α and β, respectively. Calculating the PM contribution (29) of each noise current source and multiplying by (19), the output noise of the oscillator is calculated as

$$\begin{aligned} \widehat{v_n^2} &= \left(\widehat{i^2_{\mathrm{res_{PM}}}} + \widehat{i^2_{Gn_{\mathrm{PM}}}} + \widehat{i^2_{Gp_{\mathrm{PM}}}}\right) |Z_{\mathrm{PM}}\{\omega_0 \pm \omega_m\}|^2 \\ &= 2kTR_p(1 - \alpha G_{N_{\mathrm{eff}}} R_p + \beta G_{P_{\mathrm{eff}}} R_p)\left(\frac{\omega_0}{2Q\omega_m}\right)^2 \end{aligned} \tag{62}$$

where $G_{N_{\mathrm{eff}}} = G_N[0] - G_N[2]$ and $G_{P_{\mathrm{eff}}} = G_P[0] - G_P[2]$. We can simplify further, by noting in Fig. 14 that the energy conservation requirement is now

$$G_{N_{\mathrm{eff}}} = -\left(G_{P_{\mathrm{eff}}} + \frac{1}{R_p}\right) \tag{63}$$

and so, depending on whether it is easier to calculate $G_{N_{\mathrm{eff}}}$ or $G_{P_{\mathrm{eff}}}$, we may write the noise factor as

$$\begin{aligned} F &= 1 - \alpha G_{N_{\mathrm{eff}}} R_p + \beta G_{P_{\mathrm{eff}}} R_p \\ &= (1+\alpha) + (\alpha+\beta) G_{P_{\mathrm{eff}}} R_p \\ &= (1-\beta) - (\alpha+\beta) G_{N_{\mathrm{eff}}} R_p. \end{aligned} \tag{64}$$

We now have method for investigating topologies in which the nonlinearity contributes loss to the system for some portion of the oscillation period.

B. Standard Voltage-Biased nMOS Topology

Let us apply the preceding theory to the standard voltage-biased oscillator topology shown in Fig. 15(a) that was used in early CMOS *LC* oscillators [29] for its large output amplitude. In this circuit, the transistors conduct in all three regimes: triode, saturation, off. We employ a number of simplifications to make the problem tractable. We assume the transistors adhere to the square law model, and exhibit no second-order effects such

[16]Of course, since the nonlinearity is memoryless, it can be decomposed into an arbitrary number of real-valued nonlinear resistances. However, as will be shown shortly, decomposing the nonlinearity into a positive and a negative resistance (with the associated proportional noise sources) has some physical significance.

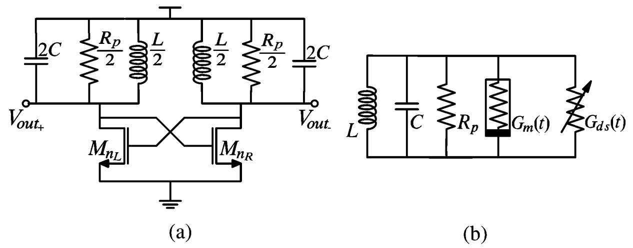

Fig. 15. Voltage-biased standard nMOS *LC* oscillator. (a) Schematic. (b) Simplified negative-gm model.

as velocity saturation. Further we assume the PSD of channel noise, i_d, across all three regions is[17]

$$\widehat{i_d^2} = 4kT(\gamma g_m + g_{\rm ds}). \tag{65}$$

1) Noise Factor: The nonlinearity in this topology arises simply from the cross-coupled differential pair. The I-V characteristic and conductance of this differential pair are plotted in Fig. 16(a). It is straightforward to show that the instantaneous conductance of the nonlinearity is given by

$$\begin{aligned} G_{\rm nr}(t) &= \frac{1}{4}(-g_{mn_R}(t) - g_{mn_L}(t) + g_{{\rm dsn}_R}(t) + g_{{\rm dsn}_L}(t)) \\ &= G_m(t) + G_{\rm ds}(t) \end{aligned} \tag{66}$$

where $G_m(t) = -(1/4)(g_{mn_R}(t) + g_{mn_L}(t))$ and $G_{\rm ds}(t) = (1/4)(g_{{\rm dsn}_R}(t) + g_{{\rm dsn}_L}(t))$. The associated noise current is given by

$$\widehat{i_{\rm nr}^2}(t) = 4kT\gamma G_m(t) + 4kTG_{\rm ds}(t) \tag{67}$$

Since the conductance of the nonlinearity is not always negative, and since its associated noise (67) is no longer proportional to the conductance (66), the general result cannot be applied. However, the nonlinearity can be decomposed into a *positive* nonlinear resistive component, $G_{\rm ds}$, and a *negative* nonlinear component, G_m, which possess the characteristics shown in Fig. 16(b). This allows us to redraw the circuit in the form of the simplified negative-gm model shown in Fig. 15(b), which is in the same general form as Fig. 14.

Intuitively, it is now possible to see why the voltage-biased oscillator is a noisy oscillator: the nonlinear positive resistance contributes loss and noise to the system; additionally the effective conductance of the system needs to be larger to overcome these losses, and therefore the noise due to G_m also increases.

Referring to (64) and (65), we note that $\alpha = \gamma$ and $\beta = 1$. Thus the output noise is

$$\widehat{v_n^2} = 2kTR_p(1+\gamma)(1 + G_{\rm DS_{eff}}R_p)\left(\frac{\omega_0}{2Q\omega_m}\right)^2 \tag{68}$$

where $G_{\rm DS_{eff}}$ takes the place of $G_{P_{\rm eff}}$ in (64). The noise factor is given by

$$\boxed{F_{\rm VB} = (1+\gamma)(1 + G_{\rm DS_{eff}}R_p).} \tag{69}$$

[17]This is a good approximation of the default SPICE2 noise model used in the BSIM3 model. As we have done throughout this work, we omit the contribution of g_{mbs}, and assume it can be accounted for in the value of γ. The more sophisticated charge based model available in BSIM3 (which is the default in the BSIM4), while more accurate, is not suitable for hand calculations.

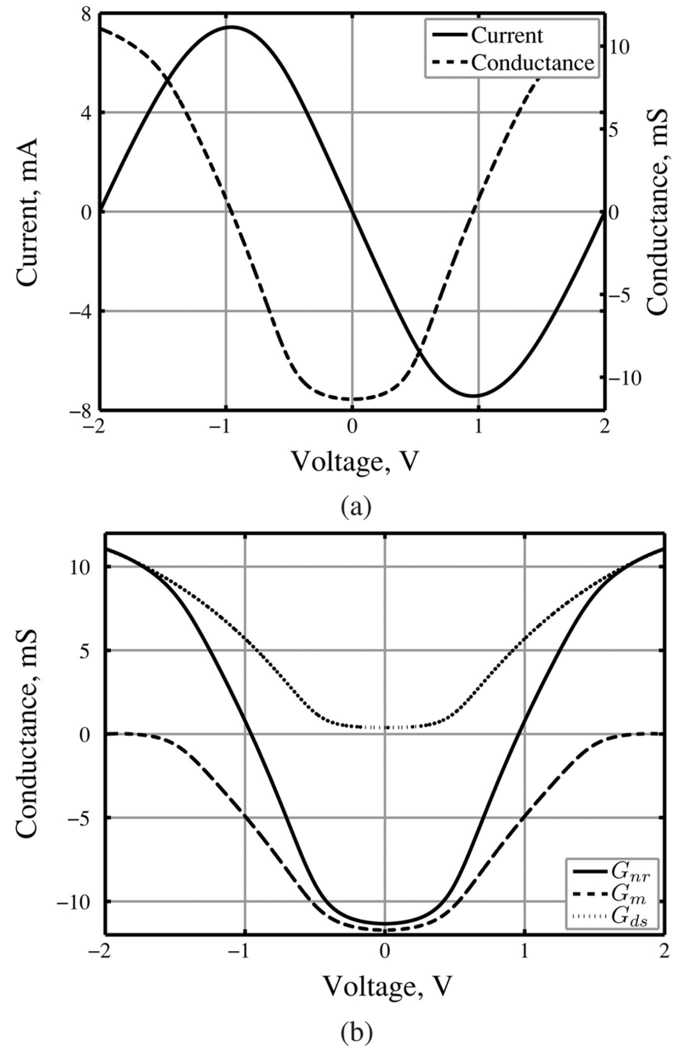

Fig. 16. Standard voltage-biased nMOS *LC* oscillator: typical plots. (a) Current and conductance characteristics. (b) Conductance characteristic decomposed as positive and negative nonlinear resistances, i.e., $G_{\rm nr} = G_m + G_{\rm ds}$.

We must now calculate $G_{\rm DS_{eff}}$. Assuming square-law transistors

$$G_{\rm ds}(t) = \begin{cases} (K/4)(V_{\rm out}(t) - V_t), & V_{\rm out}(t) \le V_t \\ (K/4)(-V_{\rm out}(t) - V_t), & V_{\rm out}(t) \le -V_t \\ 0, & \text{otherwise} \end{cases} \tag{70}$$

where $K = 0.5\mu_n C_{\rm ox} W/L$ and $V_{\rm out}(t) = A_c\cos(\omega_0 t)$. The effective positive conductance contributed by the differential pair is, therefore, calculated as

$$\begin{aligned} G_{\rm DS_{eff}} &= G_{\rm DS}[0] - G_{\rm DS}[2] \\ &= {\rm Re}\left\{\frac{K}{6A_c\pi}\left(\left(2A_c^2 + V_t^2\right)\sqrt{1 - \frac{V_t^2}{A_c^2}} \right.\right. \\ &\qquad \left.\left. - 3A_cV_t\cos^{-1}\left(\frac{V_t}{A_c}\right)\right)\right\}. \end{aligned} \tag{71}$$

Fig. 17 compares the noise factor versus oscillation amplitude for a typical voltage-biased oscillator [using (69) and (71)]

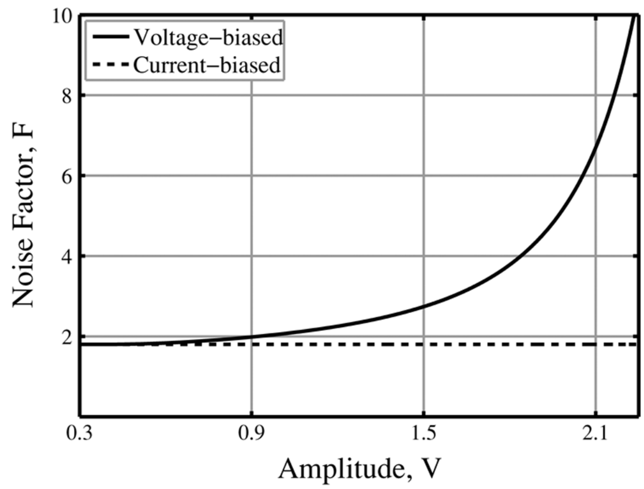

Fig. 17. Predicted noise factors of the voltage-biased and the current-biased oscillators.

and the current-biased oscillator. The noise factor of the current-biased oscillator remains constant with oscillation amplitude, while the noise factor of the voltage-biased topology rises dramatically.

2) Oscillation Amplitude: Unlike the other oscillator topologies addressed in this work, the noise factor of the voltage-biased topology depends on the oscillation amplitude; in order to calculate F, one must first calculate $G_{\mathrm{DS_{eff}}}$, which depends on A_c. A simple method to predict the oscillation amplitude of the voltage-biased topology, adapted from [30], is now presented.

In general, the amplitude of any *LC* oscillator is of the form

$$A_c = -I_{\mathrm{NR}}[1]R_p \tag{72}$$

where $I_{\mathrm{NR}}[1]$ is the first harmonic of the current drawn by the nonlinearity. How accurately we can predict the oscillation amplitude depends on how accurately we can quantify the I-V characteristic of the nonlinearity, and thus $I_{\mathrm{NR}}[1]$. In the case of the voltage-biased topology, the I-V characteristic is accurately represented using the fifth-order polynomial[18]

$$\begin{aligned} I_{\mathrm{nr}} &= g_0 V_{\mathrm{nr}} - \frac{3g_0}{8V_{dd}^2}V_{\mathrm{nr}}^3 + \frac{g_0}{32V_{dd}^4}V_{\mathrm{nr}}^5, \text{ if} \\ g_0 &= \left.\frac{\partial I_{\mathrm{nr}}}{\partial V_{\mathrm{nr}}}\right|_{V_{\mathrm{nr}}=0} \end{aligned} \tag{73}$$

with g_0 always being negative. For near sinusoidal oscillation, $V_{\mathrm{nr}} = A_c \cos(\phi)$

$$\begin{aligned} I_{\mathrm{NR}}[1] &= \frac{1}{\pi}\int_{-\pi}^{\pi} I_{\mathrm{nr}}(\phi)\cos(\phi)\,d\phi \\ &= g_0 A_c - \frac{9g_0}{32V_{dd}^2}A_c^3 + \frac{5g_0}{256V_{dd}^4}A_c^5. \end{aligned} \tag{74}$$

Substituting this value into (72) and solving for A_c gives

$$A_c = 2V_{dd}\sqrt{\frac{9}{5} - \frac{1}{5}\sqrt{1 - \frac{80}{g_0 R_p}}}. \tag{75}$$

[18]The coefficients of the polynomial are found by noting that the slope of the characteristic at $-2V_{dd}$, 0 and $2V_{dd}$ is, respectively, $-g_0$, g_0 and $-g_0$.

Simulation results suggest that this expression is a good approximation for both square law and short channel transistor models.

3) Effective, or Loaded, Q: The literature sometimes accounts for a higher than expected noise in an oscillator by pointing to an empirically fitted "effective" Q and R_p parameters, denoted as Q_{eff} and $R_{p_{\mathrm{eff}}}$, respectively. Given the above derivation, we are able to quantify these parameters. If we rewrite (68), in the form of the ideal current-biased oscillator (45)

$$\widehat{v_n^2} = 2kTR_{p_{\mathrm{eff}}}(1+\gamma)\left(\frac{\omega_0}{2Q_{\mathrm{eff}}\omega_m}\right)^2 \tag{76}$$

then we must define Q_{eff} and $R_{p_{\mathrm{eff}}}$ as

$$\begin{aligned} Q_{\mathrm{eff}} &= \frac{Q}{1+G_{\mathrm{DS_{eff}}}R_p} \\ R_{p_{\mathrm{eff}}} &= \frac{R_p}{1+G_{\mathrm{DS_{eff}}}R_p} = R_p \| \frac{1}{G_{\mathrm{DS_{eff}}}}. \end{aligned} \tag{77}$$

4) SpectreRF Simulations: The phase noise performance of the voltage-biased nMOS topology predicted by analysis was verified in SpectreRF. The oscillator was simulated using 90 nm CMOS models and a 1 V supply. An ideal linear tank with a Q of 13 and resonant frequency of 500 MHz ($\mathrm{L} = 10$ nH, $\mathrm{C} = 10.1$ pF, $\mathrm{R_p} = 400\ \Omega$) was used, while the dimensions of each finger in the differential pair were $\mathrm{W} = 3\ \mu$m, $\mathrm{L} = 0.5\ \mu$m. The amplitude was controlled by varying the number of transistor fingers from 4 to 25. Noise measurements were taken at a 100 kHz offset. Two simulations were run: one used the unaltered BSIM3v3 model card, which utilized the charge-based noise model; in a second simulation, we toggled the NOIMOD parameter of the model card to switch to the SPICE2 noise model, and increased the VSAT parameter to infinity to eliminate velocity saturation effects. Fig. 18(a) and (b) plot the simulated and predicted output PSD and phase noise of the oscillator versus amplitude. Both sets of simulation results are in good agreement with the model. As a reference, the predicted noise performance of an equivalent current-biased oscillator is also plotted. The oscillation amplitude used in theoretical predictions was obtained using (75). Notice that there is a phase noise optimum, after which, any improvement in phase noise due to a larger carrier, A_c, is negated by an increase in the noise factor, F.

C. Standard Current-Biased CMOS Topology

We now quantify, for the first time, a tank loading mechanism that can occur in all current-biased CMOS RF oscillators [11]. We demonstrate how the complementary FETs load the *LC* tank to the detriment of the noise factor *and* oscillation amplitude.

1) Noise Factor: Consider the standard current-biased CMOS topology as it is generally represented in Fig. 19(a). In the presence of a large oscillation the pMOS pair will be hard switched; for a small time around the zero-crossing both pMOS transistors will be saturated, while elsewhere one transistor will be off and the other transistor will be driven into deep triode. In this situation, current through the pMOS transistor in triode has no path to ground other than through the corresponding hard-switched nMOS transistor (via the tank). This induces a common mode oscillation on the output, which ensures that the current through both the pMOS and nMOS transistors is

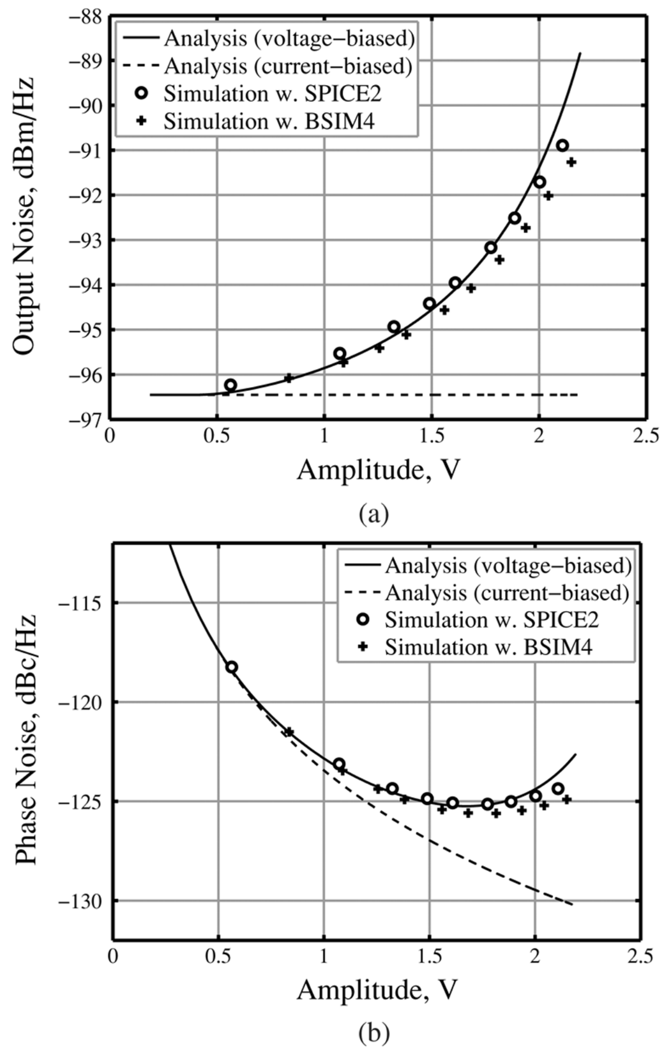

Fig. 18. Standard voltage-biased nMOS *LC* oscillator: simulation results. (a) Output noise PSD. (b) Phase noise.

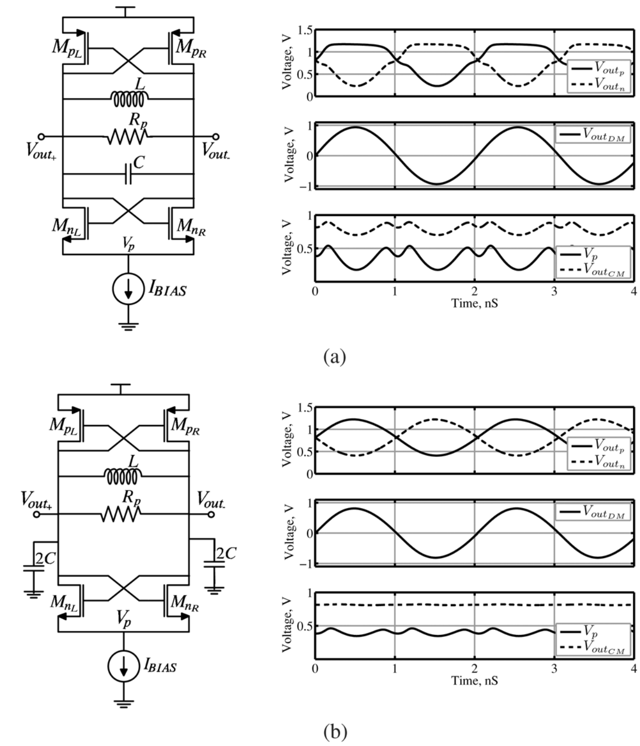

Fig. 19. Standard current-biased CMOS *LC* oscillator. (a) Fully differential capacitor arrangement. (b) Single-ended capacitor arrangement.

exactly equal to I_{BIAS} (see Fig. 19(a)). Additionally, since the current through the pMOS transistor is set by I_{BIAS}, the transistor contributes no noise while in this regime. In this case, the conductance of the nonlinearity is given by (47), the noise factor is given by $F = 1 + \gamma$ and the oscillation amplitude is given by $A_c = (4/\pi) I_{\mathrm{BIAS}} R_p$.

However, if the tank capacitance does not appear across the tank, but rather as two single-ended capacitors connected to ground [see Fig. 19(b)], the oscillator will behave very differently [11]. This is, in fact, generally the situation at RF, when the resonator is made up of an on-chip spiral inductor tuned by the capacitances to ground at the drain junctions and at the pMOS gates, with only the nMOS gates offering a small portion of the total capacitance that floats in parallel with the inductor. If the single-ended capacitors are sufficiently large, they can suppress the common mode oscillation, as shown in Fig. 19(b), and the current through a hard-switched pMOS transistor will have two paths to ground: through the corresponding hard-switched nMOS transistor and through the capacitors. In this instance, the oscillator is more appropriately viewed as a *voltage-biased pMOS* pair [as in Fig. 15(a)], in parallel with the hard-limiting nonlinearity provided by the *current-biased nMOS* pair. Now the time-varying conductance is given by

$$\begin{aligned} G_{\mathrm{nr}}(t) &= -\left[\frac{g_{mn_R}(t) g_{mn_L}(t)}{g_{mn_R}(t) + g_{mn_L}(t)}\right] \\ &\quad - \left[\frac{1}{4}\left(g_{mp_R}(t) + g_{mp_L}(t)\right)\right] \\ &\quad + \left[\frac{1}{4}\left(g_{\mathrm{dsp}_R}(t) + g_{\mathrm{dsp}_L}(t)\right)\right] \\ &= G_{m_n}(t) + G_{m_p}(t) + G_{\mathrm{ds}_p}(t). \end{aligned} \tag{78}$$

Here we have three nonlinear conductances: a *negative* conductance, $G_{m_n}(t)$, due to the current-biased nMOS differential pair, a *negative* conductance, $G_{m_p}(t)$, due to the transconductance of the pMOS transistors, and a *positive* conductance, $G_{\mathrm{ds}_p}(t)$, due to the drain-source conductance of the pMOS transistors. If we lump together $G_{m_n}(t)$ and $G_{m_p}(t)$ as a single negative nonlinear resistor, the noise factor of the oscillator can be obtained in the same way as the noise factor of the voltage-biased topology (see in Section VII-B). Working through the calculations the output PSD is found to be

$$\widehat{v_n^2} = 2kTR_p(1+\gamma)(1 + G_{\mathrm{DS_{EFF}}} R_p)\left(\frac{\omega_0}{2Q\omega_m}\right)^2 \tag{79}$$

where the effective conductance, $G_{\mathrm{DS_{EFF}}}$, responsible for tank loading, is given by

$$\begin{aligned} G_{\mathrm{DS_{EFF}}} &= G_{\mathrm{DS}}[0] - G_{\mathrm{DS}}[2] \\ &= \mathrm{Re}\left\{\frac{K}{6A_c\pi}\left(\left(2A_c^2 + V_{t_p}^2\right)\sqrt{1 - \frac{V_{t_p}^2}{A_c^2}}\right.\right. \\ &\quad \left.\left. + 3A_c V_{t_p}\cos^{-1}\left(\frac{|V_{t_p}|}{A_c}\right)\right)\right\}. \end{aligned} \tag{80}$$

Again, this expression assumes the tank capacitance is single-ended and the common-mode oscillation is completely suppressed. The noise factor then equals

$$\boxed{F_{\mathrm{CMOS_{loaded}}} = (1+\gamma)(1+G_{\mathrm{DS_{EFF}}}R_p)} \tag{81}$$

and this depends on both biasing and technology.

2) Oscillation Amplitude: When the tank capacitors are tied to ground, the oscillation amplitude is no longer given by $A_c = (4/\pi)I_{\mathrm{BIAS}}R_p$. Instead, we derive the amplitude by calculating the fundamental of the current drawn by the nMOS pair and the voltage-biased pMOS pair, summing the result, and multiplying by $-R_p$. The current-biased nMOS pair draws a differential current whose fundamental component is approximately

$$I_{\mathrm{NR_{nMOS}}}[1] = -\frac{2}{\pi}I_{\mathrm{BIAS}} \tag{82}$$

while the voltage-biased pMOS pair draws a differential current whose fundamental component is

$$I_{\mathrm{NR_{pMOS}}}[1] = g_{0_p}A_c - \frac{9g_{0_p}}{32V_{\mathrm{DG}_p}^2}A_c^3 + \frac{5g_{0_p}}{256V_{\mathrm{DG}_p}^4}A_c^5 \tag{83}$$

where $V_{DG_p} = V_{dd} - V_{\mathrm{out_{CM}}}$, and g_{0_p} is conductance of the differential pMOS pair $(-g_{mp}/2)$ measured at DC. This expression is derived by modeling the pMOS nonlinearity as a 5th-order polynomial[19], as was done in Section VII-B. The oscillation amplitude is therefore calculated by finding the appropriate root of the implicit equation

$$\begin{aligned} A_c &= -(I_{\mathrm{NR_{nMOS}}}[1] + I_{\mathrm{NR_{pMOS}}}[1])R_p \\ &= \left(\frac{2}{\pi}I_{\mathrm{BIAS}} - g_{0_p}A_c + \frac{9g_{0_p}A_c^3}{32V_{\mathrm{DG}_p}^2} - \frac{5g_{0_p}A_c^5}{256V_{\mathrm{DG}_p}^4}\right)R_p. \end{aligned} \tag{84}$$

Numerical methods are required to solve for A_c.

3) SpectreRF Simulations: The predicted noise performance of the CMOS voltage-biased topology, for the two capacitor arrangements discussed, was verified in SpectreRF. The oscillator was simulated using 90 nm models, a 1.2 V supply, and an ideal noiseless current source. An ideal linear tank with a Q of 19 and a resonant frequency of 500 MHz (L = 5 nH, C = 20.2 pF, $\mathrm{R_P}$ = 300 Ω) was used. The dimensions of the differential nMOS and pMOS pair fingers were W = 1.5 μm, L = 0.2 μm. The nMOS transistors had 50 fingers while the pMOS transistor had 225. Fig. 20 plots the simulated and predicted phase noise of the two topologies, measured at a 100 kHz offset. The simulated and predicted amplitudes are plotted in Fig. 21 and are in good agreement. The predicted and simulated results diverge once the amplitude of oscillation reaches the rail voltage.

The results presented here show a substantial degradation in both amplitude and noise-performance, while the extent of this degradation depends on the size, biasing and technology parameters of the pMOS transistors.

[19]If there were no grounded capacitors, the differential current drawn by the pMOS transistors would equal $-(2/\pi)I_{\mathrm{BIAS}}$.

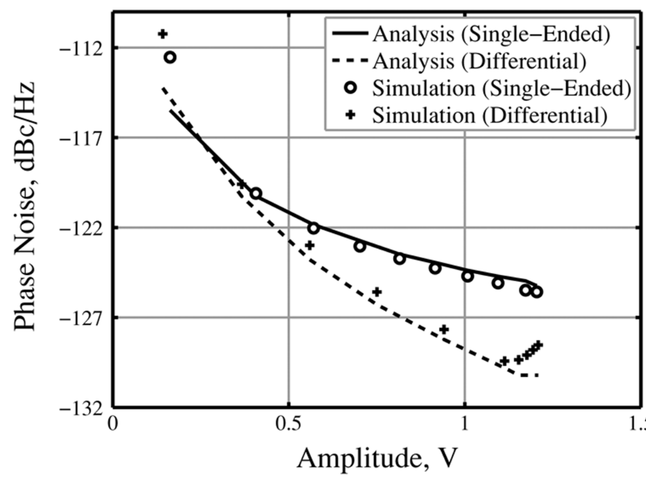

Fig. 20. Phase noise performance of the CMOS standard current-biased *LC* topology with a differential capacitor arrangement and a single-ended capacitor arrangement.

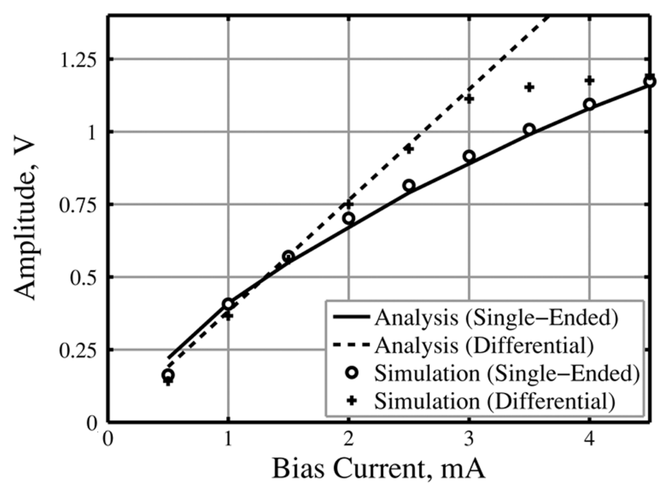

Fig. 21. Amplitude of the CMOS standard current-biased *LC* topology with a differential capacitor arrangement and a single-ended capacitor arrangement.

VIII. Conclusion

Using a phasor-based analysis method, we have re-derived the general result presented by Banks [14], and Mazzanti and Andreani [15]. With only a few steps, this can predict phase noise in a range of popular oscillator circuits and guide their optimal design. The phasor-based analysis also leads to simple expressions for amplitude noise in *LC* oscillators. The analysis sheds new light on the loaded Q of oscillators, in particular on the widely used fully differential CMOS *LC* oscillator.

We show that the two competing methods of phase noise analysis today, ISF and phasor-based, are, in fact, equivalent.

Appendix A
Reconciling the ISF and Phasor-Based Approaches

To truly reconcile the two approaches, we consider a small single-tone current, shaped by an arbitrary waveform, and injected into the negative-gm model (see Fig. 4). We assume the injected tone is of the form $i_k(t) = I_N\cos((k\omega_0 + \omega_m)t + \phi)$, and is modulated by the function $w(t)$. Using the approach laid out in this work, the power in the resulting PM sideband is

$$\begin{aligned} P_{\text{phasor}}\{\omega_m\} &= \mathcal{S}_{\text{PM}}\{k\}|Z_{\text{PM}}|^2 \\ &= \left(\frac{I_N^2}{8}\right)|W[-k+1]-W[-k-1]|^2|Z_{\text{PM}}|^2. \end{aligned} \tag{85}$$

This is simply the PM component of $i_k(t)$ [see (25)], multiplied by the PM transfer function given by (19). On the other hand, Hajimiri and Lee's approach shows that the power in the resulting PM sideband is given by

$$\begin{aligned} P_{\text{ISF}}\{\omega_m\} &= \frac{A^2}{2}\left(\frac{I_n|\Gamma_{\text{eff}}[k]|}{2q_{\max}\omega_m}\right)^2 \\ &= \frac{(I_n|\Gamma_{\text{eff}}[k]|)^2}{2}\left(\frac{\omega_0}{2Q\omega_m}\right)^2 R_p^2, \\ &= \frac{(I_n|\Gamma_{\text{eff}}[k]|)^2}{2}|Z_{\text{PM}}|^2 \end{aligned} \tag{86}$$

where $q_{\max} = CA_c$, $\Gamma_{\text{eff}}(t) = \Gamma(t)\text{NTF}(t)$ and $\Gamma(t)$ is the ISF. Hajimiri and Lee's noise-transfer function (NTF) is the same as our noise-shaping function $w(t)$. Andreani and Wang [31] make the approximation that, in a nearly-sinusoidal oscillator, if the output is of the form $V_{\text{out}}(x) = A_c\cos(x)$, the ISF is given by $\Gamma(x) = -\sin(x)$. Using this approximation, the effective ISF Fourier coefficients are given by

$$\begin{aligned} \Gamma_{\text{rms}}[k] &= \frac{1}{T}\int_{T/2}^{-T/2} w(t)\Gamma(\omega_o t)\mathrm{e}^{-jk\omega_o t}\,dt \\ &= \frac{j}{2}(W[k-1]-W[k+1]). \end{aligned} \tag{87}$$

Therefore

$$P_{\text{ISF}}\{\omega_m\} = \left(\frac{I_n}{8}\right)^2 |W[k-1]-W[k+1]|^2|Z_{\text{PM}}|^2 \tag{88}$$

which is exactly the same as the expression obtained using the phasor-based approach (85). Again, unlike the phasor approach, the ISF has not yet been used to develop a closed form expression for AM sidebands.

Given the above analysis, the parallels between the two approaches are as follows: our noise-shaping function $w(t)$ is identical to Hajimiri and Lee's NTF; the phasor decomposition of the sidebands around the carrier frequency (see Section IV) performs the same operation as the ISF, $\Gamma(x) = -\sin(x)$; and the preservation of the PM sideband-to-carrier ratio through the nonlinearity (Section III-B), takes the place of the unit step in Hajimiri and Lee's phase impulse response function.

Appendix B
NMOS Differential Pair: Conductance and Noise

Consider the differential pair in Fig. 11(b). If we assume square law models, and V_{nr} is small enough that both transistors remain in saturation, we can write

$$\begin{aligned} I_L &= \frac{1}{2}\mu_n\frac{W_L}{L_L}C_{\text{ox}}(V_{\text{GS}_L}-V_{t_L})^2 \\ I_R &= \frac{1}{2}\mu_n\frac{W_R}{L_R}C_{\text{ox}}(V_{\text{GS}_R}-V_{t_R})^2 \end{aligned} \tag{89}$$

where $V_{\text{GS}_L} = V_{\text{DD}} - V_{\text{nr}}/2 - V_{\text{CM}}$, $V_{\text{GS}_R} = V_{\text{DD}} + V_{\text{nr}}/2 - V_{\text{CM}}$, $I_{\text{BIAS}} = I_L + I_R$, $I_{\text{NR}} = (I_L - I_R)/2$, and V_{CM} is the source voltage of each transistor. Further

$$g_{mn_R} = \frac{\partial I_L}{\partial V_{\text{GS}_L}}; g_{mn_L} = \frac{\partial I_R}{\partial V_{\text{GS}_R}}; G_m = \frac{\partial I_{\text{NR}}}{\partial V_{\text{nr}}}. \tag{90}$$

Solving for G_m in terms of g_{mn_R} and g_{mn_L} results in (43). If the V_{nr} is large enough that the pair is fully-switched, the transconductance of each transistor (and the conductance of the differential pair) drops to zero and (43) remains valid. Furthermore, since the pair will be fully-switched before at least one transistor drops into triode, (43) is valid for all regions of operation.

When both transistor are saturated, we can associated the noise currents $\widehat{i_{n_L}^2} = 4kT\gamma g_{mn_L}$ and $\widehat{i_{n_R}^2} = 4kT\gamma g_{mn_R}$ to the appropriate transistors. The resulting differential noise current is

$$\begin{aligned} \widehat{i_{\text{nr}}^2} &= \frac{1}{2}\left(\widehat{i_{n_R}^2}\frac{g_{mn_L}}{g_{mn_L}+g_{mn_R}} + \widehat{i_{n_R}^2}\frac{g_{mn_L}}{g_{mn_L}+g_{mn_R}}\right) \\ &= 4kT\gamma\frac{g_{mn_L}g_{mn_R}}{g_{mn_L}+g_{mn_R}} \end{aligned} \tag{91}$$

which is equivalent to (44). When fully-switched, the pair contributes no noise and so (44) remains valid in all regions.

A similar analysis can be carried out for the CMOS differential pair, which results in (47) and (48).

References

[1] D. B. Leeson, "A simple model of feedback oscillator noise spectrum," *Proc. IEEE*, vol. 54, no. 2, pp. 329–330, Feb. 1966.

[2] F. X. Kaertner, "Determination of the correlation spectrum of oscillators with low noise," *IEEE Trans. Microw. Theory Tech.*, vol. 37, no. 1, pp. 90–101, Jan. 1989.

[3] A. Demir, A. Mehrotra, and J. Roychowdhury, "Phase noise in oscillators: A unifying theory and numerical methods for characterization," *IEEE Trans. Circuits Syst. I, Fundam. Theory Appl.*, vol. 47, no. 5, pp. 655–674, May 2000.

[4] A. Demir, "Phase noise and timing jitter in oscillators with colored-noise sources," *IEEE Trans. Circuits Syst. I, Fundam. Theory Appl.*, vol. 49, no. 12, pp. 1782–1791, Dec. 2002.

[5] A. Hajimiri and T. H. Lee, "A general theory of phase noise in electrical oscillators," *IEEE J. Solid-State Circuits*, vol. 33, no. 2, pp. 179–194, Feb. 1998.

[6] A. Hajimiri and T. H. Lee, "Corrections to "a general theory of phase noise in electrical oscillators"," *IEEE J. Solid-State Circuits*, vol. 33, no. 6, pp. 928–928, Jun. 1998.

[7] C. Samori, A. L. Lacaita, F. Villa, and F. Zappa, "Spectrum folding and phase noise in LC tuned oscillators," *IEEE Trans. Circuits Syst. II, Analog Digit. Signal Process.*, vol. 45, no. 7, pp. 781–790, Jul. 1998.

[8] Q. Huang, "Phase noise to carrier ratio in LC oscillators," *IEEE Trans. Circuits Syst. I, Fundam. Theory Appl.*, vol. 47, no. 7, pp. 965–980, Jul. 2000.

[9] J. J. Rael and A. A. Abidi, "Physical processes of phase noise in differential LC oscillators," in *Proc. IEEE Custom Integr. Circuits Conf. (CICC)*, 2000, pp. 569–572.

[10] P. Andreani, X. Wang, L. Vandi, and A. Fard, "A study of phase noise in Colpitts and LC-tank CMOS oscillators," *IEEE J. Solid-State Circuits*, vol. 40, no. 5, pp. 1107–1118, May 2005.

[11] P. Andreani and A. Fard, "More on the $1/f^2$ phase noise performance of CMOS differential-pair LC-tank oscillators," *IEEE J. Solid-State Circuits*, vol. 41, no. 12, pp. 2703–2712, Dec. 2006.

[12] A. Fard and P. Andreani, "An analysis of $1/f^2$ phase noise in bipolar Colpitts oscillators (with a digression on bipolar differential-pair LC oscillators)," *IEEE J. Solid-State Circuits*, vol. 42, no. 2, pp. 374–384, Feb. 2007.

[13] P. Andreani and A. Fard, "A 2.3 GHz LC-tank CMOS VCO with optimal phase noise performance," in *Proc. Int. Solid-State Circuits Conf. (ISSCC)*, Feb. 2006, pp. 691–700.
[14] J. Bank, "A harmonic-oscillator design methodology based on describing functions," Ph.D. dissertation, Dept. Signals Syst., Sch. Elect. Eng., Chalmers Univ. Techn., Chalmers, Sweden, 2006.
[15] A. Mazzanti and P. Andreani, "Class-C harmonic CMOS VCOs, with a general result on phase noise," *IEEE J. Solid-State Circuits*, vol. 43, no. 12, pp. 2716–2729, Dec. 2008.
[16] K. A. Kouznetsov and R. G. Meyer, "Phase noise in LC oscillators," *IEEE J. Solid-State Circuits*, vol. 35, no. 8, pp. 1244–1248, Aug. 2000.
[17] E. Hegazi, J. J. Rael, and A. A. Abidi, *The Designer's Guide to High-Purity Oscillators*. New York: Springer, 2004.
[18] J. Phillips and K. Kundert, "Noise in mixers, oscillators, samplers, and logic an introduction to cyclostationary noise," in *Proc. IEEE Custom Integr. Circuits Conf. (CICC)*, 2000, pp. 431–438.
[19] J. Rael, "Phase noise in LC oscillators," Ph.D. dissertation, Elect. Eng. Dept., Univ. California, Los Angeles, 2007.
[20] E. Hegazi and A. A. Abidi, "Varactor characteristics, oscillator tuning curves, and AM-FM conversion," *IEEE J. Solid-State Circuits*, vol. 38, no. 6, pp. 1033–1039, Jun. 2003.
[21] W. P. Robins, *Phase Noise in Signal Sources: Theory and Applications*. London, U.K.: Institution of Electrical Engineers, 1984.
[22] H. Darabi and A. A. Abidi, "Noise in RF-CMOS mixers: A simple physical model," *IEEE J. Solid-State Circuits*, vol. 35, no. 1, pp. 15–25, Jan. 2000.
[23] E. Hegazi, H. Sjoland, and A. A. Abidi, "A filtering technique to lower LC oscillator phase noise," *IEEE J. Solid-State Circuits*, vol. 36, no. 12, pp. 1921–1930, Dec. 2001.
[24] H. Wang, "A solution for minimizing phase noise in low-power resonator-based oscillators," in *Proc. IEEE Int. Symp. Circuits Syst. (ISCAS)*, 2000, vol. 3, pp. 53–56.
[25] A. Mazzanti and P. Andreani, "A 1.4 mW 4.90-to-5.65 GHz class-C CMOS VCO with an average FoM of 194.5 dBc/Hz," in *Proc. Int. Solid-State Circuits Conf. (ISSCC)*, Feb. 2008, pp. 474–629.
[26] S. Shekhar, J. Walling, S. Aniruddhan, and D. Allstot, "CMOS VCO and LNA using tuned-input tuned-output circuits," *IEEE J. Solid-State Circuits*, vol. 43, no. 5, pp. 1177–1186, May 2008.
[27] B. Soltanian and P. Kinget, "Tail current-shaping to improve phase noise in LC voltage-controlled oscillators," *IEEE J. Solid-State Circuits*, vol. 41, no. 8, pp. 1792–1802, Aug. 2006.
[28] T. H. Lee, *The Design of CMOS Radio-Frequency Integrated Circuits*, 2nd ed. Cambridge, U.K.: Cambridge University Press, 2003.
[29] A. Rofougaran, G. Chang, J. Rael, J.-C. Chang, M. Rofougaran, P. Chang, M. Djafari, M.-K. Ku, E. Roth, A. Abidi, and H. Samueli, "A single-chip 900-MHz spread-spectrum wireless transceiver in 1-μm CMOS. I. Architecture and transmitter design," *IEEE J. Solid-State Circuits*, vol. 33, no. 4, pp. 515–530, 1998.
[30] D. Murphy, M. P. Kennedy, J. Buckley, and M. Qu, "The optimum power conversion efficiency and associated gain of an LC CMOS oscillator," in *Proc. IEEE Int. Symp. Circuits Syst. (ISCAS)*, May 2006, pp. 2633–2636.
[31] P. Andreani and X. Wang, "On the phase-noise and phase-error performances of multiphase LC CMOS VCOs," *IEEE J. Solid-State Circuits*, vol. 39, no. 11, pp. 1883–1893, Nov. 2004.

David Murphy received the B.E. and M.Eng.Sc. degrees from the National University of Ireland, Cork, in 2004 and 2006, respectively. He is currently pursuing the Ph.D. degree from the University of California, Los Angeles.

Jacob J. Rael (S'93-M'99) received the S.B. degree from the Massachusetts Institute of Technology, Boston, in 1991, and the M.S. and Ph.D. degrees in electrical engineering from the University of California, Los Angeles, CA, in 1995 and 2007, respectively.

In 1998, he joined Innovent Systems which was acquired by Broadcom Corporation, Irvine, CA., in 2000, where he is currently a Manager. His research interests include CMOS RF design and design automation.

Dr. Rael was a corecipient of the Jack Kilby Best Student Paper Award at the 1996 ISSCC, the Jack Raper Award for Outstanding Technology Directions Paper at the 1997 ISSCC, and the Design Contest Award at the 1998 Design Automation Conference. He is the Chairman of the Los Angeles Chapter of the Solid State Circuits Society.

Asad A. Abidi (S'75-M'80-SM'95-F'96) received the B.Sc. degree (with honors) from Imperial College, London, U.K., in 1976 and the M.S. and Ph.D. degrees in electrical engineering from the University of California, Berkeley, in 1978 and 1981, respectively.

From 1981 to 1984, he was with Bell Laboratories, Murray Hill, NJ, as a Member of the Technical Staff with the Advanced LSI Development Laboratory. Since 1985, he has been with the Department of Electrical Engineering, University of California, Los Angeles, where he is currently a Professor. He was a Visiting Faculty Researcher with Hewlett-Packard Laboratories in 1989. His research interests include RF CMOS design, high-speed analog integrated circuit design, data conversion, and other techniques of analog signal processing.

Dr. Abidi was a recipient of an IEEE Millennium Medal, the 1988 TRW Award for Innovative Teaching, and the 1997 IEEE Donald G. Fink Award, and he was a corecipient of the Best Paper Award at the 1995 European Solid-State Circuits Conference, the Jack Kilby Best Student Paper Award at the 1996 ISSCC, the Jack Raper Award for Outstanding Technology Directions Paper at the 1997 ISSCC, the Design Contest Award at the 1998 Design Automation Conference, an Honorable Mention at the 2000 Design Automation Conference, and the 2001 ISLPED Low Power Design Contest Award. He was the Program Secretary for the IEEE International Solid-State Circuits Conference (ISSCC) from 1984 to 1990 and the General Chairman of the Symposium on VLSI Circuits in 1992. He was the Secretary of the IEEE Solid-State Circuits Council from 1990 to 1991. From 1992 to 1995, he was an Editor for the IEEE JOURNAL OF SOLID-STATE CIRCUITS. He was named one of the top ten contributors to the ISSCC. He has been elected to the National Academy of Engineering.